AGU PUBLICATIONS

JGR

Journal of Geophysical Research: Solid Earth

RESEARCH ARTICLE

10.1002/2013JB010504

Key Points:
- Ocean waves force seabed pressure fluctuations with three spectral peaks
- These spectral peaks match the spectrum of seismic noise observations
- Simulations show typical waves generate all three of these peaks

Correspondence to:
J. Traer,
jtraer@mit.edu

Citation:
Traer, J., and P. Gerstoft (2014), A unified theory of microseisms and hum, *J. Geophys. Res. Solid Earth*, *119*, 3317–3339, doi:10.1002/2013JB010504.

Received 9 JUL 2013
Accepted 11 MAR 2014
Accepted article online 15 MAR 2014
Published online 23 APR 2014

A unified theory of microseisms and hum

James Traer[1] and Peter Gerstoft[2]

[1]Department of Brain and Cognitive Sciences, Massachusetts Institute of Technology, Cambridge, Massachusetts, USA, [2]Marine Physical Laboratory, Scripps Institution of Oceanography, University of California, San Diego, La Jolla, California, USA

Abstract Interacting ocean surface waves force water column pressure fluctuations with spectral peaks at the same frequencies of primary microseisms (PM), double-frequency microseisms (DF), and seismic hum. Prior treatment of nonlinear ocean wave interactions has focused on the DF pressure fluctuations which, in the presence of opposing waves, do not decay with depth and hence are dominant in deep waters. For an arbitrary 2-D surface wave spectrum we integrate over all pairings of wave vectors, directions, and frequencies to obtain a full-spectrum perturbation expansion including the first- and second-order pressure waves. First-order pressure waves generate a peak at PM frequencies and second-order pressure waves generated by obliquely interacting surface waves generate pressure fluctuations at DF and hum frequencies. These pressure fluctuations decay with depth but interact with the seabed in shallow water. As their generation does not require precise wave states, they are likely ubiquitous in shallow water.

1. Introduction

Microseisms and the Earth's hum are seismic signals generated by ocean waves. Although much weaker than earthquakes they are observed to be continuous and ubiquitous. Recently, there have been significant efforts to model the oceanic regions of microseism generation based on ocean wave hindcasts [*Kedar et al.*, 2008; *Ardhuin et al.*, 2011, 2012; *Stutzmann et al.*, 2012; *Hillers et al.*, 2012; *Obrebski et al.*, 2012; *Ardhuin and Herbers*, 2013; *Obrebski et al.*, 2013]. These models may allow for better understanding of microseisms and improved seismic tomography, as the source regions can be constrained by easily accessible ocean surface wave measurements. These microseism models are based on the *Longuet-Higgins* [1950]; *Hasselmann* [1963] model in which standing waves are created by nearly opposing wavefields. Such models have shown good results at twice the ocean wave peak-frequency, but they do not address shallow-water microseism generation where evanescent ocean waves interact with complex sea bottom topography. Thus, they may underestimate microseism generation in shallow water [*Hillers et al.*, 2012].

To generate microseisms and hum on land requires two steps: (1) ocean surface waves generate pressure fluctuations at the seabed; which then (2) excite propagating seismic waves in the earth. We consider the first step using a perturbation procedure [*Hasselmann*, 1963] to compute the full wave-induced pressure at the seafloor in shallow water. The entire gravity wave spectrum is considered, including all second-order components. We show that the seabed pressure spectrum in shallow water has peaks at the same frequencies as ambient seismic noise. Although the coupling of the seabed pressure to seismic waves is not modeled, the fact that one of the observed microseism peaks has the same frequency as ocean waves suggests that seabed pressure waves can linearly excite seismic waves of the same frequency. Presumably, the other peaks in the seabed pressure spectrum excite seismic waves via this mechanism. A linear coupling such as this was proposed by *Hasselmann* [1963] but has not been modeled in the same detail as standing waves. Observations of microseisms at ocean wave frequencies are ubiquitous and a significant fraction of observed microseisms may be generated in this way.

The spectrum of ocean wave-induced seismicity contains three peaks [*Webb*, 1992, 2007]. The most energetic peak is at double the frequency of ocean waves, the double-frequency (DF) microseism peak. Nearly opposing waves of the same frequency generate standing waves at double the frequency of the initial waves [*Longuet-Higgins*, 1950; *Hasselmann*, 1963] with energy independent of depth, while ocean surface gravity waves decay exponentially with depth. The DF standing waves have very small wave numbers and thus couple efficiently to seismic modes that have lower wave numbers than ocean surface waves.

A smaller peak, the primary microseism (PM) peak, is centered at the frequency of ocean surface waves. This peak is attributed to the direct interaction of ocean waves with the seabed. Although the ocean surface

waves have much higher wave numbers than the seismic modes they excite, in environments with varying ocean depth the ocean wave spectrum varies spatially and can excite low-wave number fluctuations in the seabed [*Hasselmann*, 1963]. As ocean waves decay exponentially with depth, this generation process is limited to shallow water; however, the average observed primary microseism peak is only 20 dB less than the DF peak [*Webb*, 2007] and thus represents a significant fraction of observed microseism energy.

The smallest peak, the Earth's seismic hum, is centered at frequencies much lower than those of ocean surface gravity waves [*Kobayashi and Nishida*, 1998; *Suda et al.*, 1998; *Tanimoto et al.*, 1998; *Nishida and Kobayashi*, 1999; *Rhie and Romanowicz*, 2004, 2006; *Tanimoto*, 2005; *Webb*, 2007, 2008; *Tanimoto*, 2008; *Romanowicz*, 2010; *Bromirski and Gerstoft*, 2009; *Fukao et al.*, 2010; *Nishida*, 2013]. The Earth's seismic hum is usually attributed to infragravity waves, ocean waves of exceptionally low frequency that are generated by the interactions of ocean surface-gravity waves with the seabed in shallow water [*Herbers et al.*, 1995]. The Earth's hum has been considered a distinct process from microseisms (DF and PM) and most theoretical and observational work has considered them separately.

Observations of seabed pressure have observed fluctuations at DF frequencies on the deep seafloor [*Wilson et al.*, 2003; *Bromirski et al.*, 2005; *Harmon et al.*, 2007; *Farrell and Munk*, 2008], and *P* wave microseisms have been observed to be generated somewhat uniformly across all water depths [*Haubrich and McCamy*, 1969; *Gerstoft et al.*, 2008; *Koper et al.*, 2010; *Zhang et al.*, 2010; *Landès et al.*, 2010; *Hillers et al.*, 2012]. Observations of seabed pressure in shallow water have revealed, in addition, pressure fluctuations at DF frequencies that decay exponentially with depth [*Cox and Jacobs*, 1989; *Herbers and Guza*, 1991, 1992, 1994]. The interaction of these vertically evanescent waves with the seabed in shallow waters has not been modeled much, and thus, it is not known to what extent they contribute to observed DF microseisms. Correlation of both DF microseism [*Bromirski et al.*, 2005; *Traer et al.*, 2012] and hum [*Bromirski and Gerstoft*, 2009] energy with ocean wave energy shows high correlation in coastal waters, suggesting that much of the DF microseisms and hum observed on land are generated in shallow waters where evanescent signals interact with the seabed.

Detailed solutions of compressible equations in the water and atmosphere yield propagating low-frequency acoustic modes in the ocean [*Kuperman and Ingenito*, 1980; *Cato*, 1991a; *Wilson et al.*, 2003; *Traer et al.*, 2008; *Brooks and Gerstoft*, 2009; *Farrell and Munk*, 2010; *Duennebier et al.*, 2012] and atmospheric microbaroms [*Waxler and Gilbert*, 2006; *Landès et al.*, 2012; *Hedlin et al.*, 2012; *Walker*, 2012] which have been modeled in detail. However, these models are exceedingly complicated and, in order to make the algebra tractable, they focus on the propagating modes and neglect evanescent solutions. This paper differs from most prior wave interaction models in that it (1) computes a full integration over the space of all possible interacting ocean surface waves rather than just the opposing waves and (2) includes rapidly decaying evanescent fluctuations. Initially, we neglect compressibility of the water column, to give greatly simplified governing equations. This simplification allows the full integration to become tractable; it does not, however, include propagating seismic or acoustic modes [*Cato*, 1991a, 1991b; *Kibblewhite and Wu*, 1996] but only elliptical motions of the water and seabed, analogous to ocean surface waves. Later, compressibility is included, and we see that only in the standing wave case, where the wave number is very small, are the results much different. Thus, a fully integrated ocean surface wavefield yields both propagating acoustic modes, which have been modeled extensively, and vertically evanescent elliptical motions of the water column, similar to those that excite PM [*Hasselmann*, 1963]. These have been observed [*Cox and Jacobs*, 1989; *Herbers and Guza*, 1991, 1992, 1994] at DF frequencies but have not been modeled in detail as microseism sources.

The theory presented quantifies the energy of seabed pressure fluctuations induced by the evanescent waves, relative to that of the standing waves at DF frequencies, and shows peaks at the same frequencies as observations of seismic noise (hum, PM, and DF). Although evanescent waves are only important in shallow water, their generation does not require opposing waves. Indeed, given the broad directionality of ocean waves, the pressure fluctuations described here are likely ubiquitous.

2. Theoretical Overview

In the following we describe how quadratic interactions between two ocean surface waves yield second-order waves with frequencies at the sum and difference values of the two initial waves (section 2.1). The second-order pressure due to wave-induced motion in the water column is derived first within an incompressible fluid (section 3). This simple model demonstrates the underlying physics of the wave-wave

Table 1. Notational Conventions Used

Notation	Definition
	Basic Terms
$\mathbf{x} = (x, y, z)^{\mathsf{T}}$, t	Coordinates; $z = 0$ at the surface and positive downward, time
g, ρ, H, c	Gravitational acceleration, water density, depth of the seabed, water column sound speed
$\zeta(x, y)$	Vertical displacement of the ocean surface
$P(\mathbf{x}, t)$	Pressure at point $\mathbf{x}$ and time t
$\mathbf{v}(\mathbf{x}, t)$	Velocity of fluid particles at $\mathbf{x}$ and time t
$\Phi(\mathbf{x}, t)$	Velocity potential at point $\mathbf{x}$ and time t, such that $\mathbf{v} = \nabla\Phi$
Z, Ξ, Z^0, Z', Ξ^0, Ξ'	Depth dependance in incompressible and compressible fluids. The superscript ^{0} indicates the value at the ocean surface $Z(z=0)$, and $'$ indicates the first derivative evaluated at the surface $\partial Z/\partial z\vert_{z=0}$
$\check{Z}$, $\check{\Xi}$	Depth-dependent functions that are the product of two depth dependancies evaluated at different wave numbers $\check{Z} = Z_1 Z_2$
D, Θ	Functions that scale the amplitude of second-order solutions by wave number, frequency and angular separation of the interacting first-order waves
$S_{\pm}(\mathbf{k}, \omega)$, $\check{S}_{\pm}(\mathbf{k}, \omega)$	Integral terms using δ functions to sift possible combinations of *first-order* contributions that yield a combined wave vector and frequency of $\mathbf{k}$ and ω
	Perturbation Expansion
$\mathbf{q} = (q_x, q_y, q_z)^{\mathsf{T}}$	Wave number of the spectral components of the *first-order* solutions
$\mathbf{k} = (k_x, k_y, k_z)^{\mathsf{T}}$	Wave number of the spectral components of the *second-order* solutions
σ, ω	Frequency of the first σ and second-order ω solutions
σ_q	σ computed from the first-order dispersion relation for a particular value of $\vert\mathbf{q}\vert$
$P^{(j)}$, $\Phi^{(j)}$, $\zeta^{(j)}$	jth term ($j \in \{1, 2\}$) of the perturbation expansion of P, Φ, ζ
$\xi_{q\sigma}$, $\xi_{k\omega}$	Time- and space-dependent phase $\xi_{q\sigma} = \mathbf{q}^T\mathbf{x} - \sigma t$, $\xi_{k\omega} = \mathbf{k}^T\mathbf{x} - \omega t$
	Fourier Transform
$\eta_{q\sigma}$, $a_{q\sigma}$	Spectral components of $\zeta^{(1)}$ after Fourier decomposition using $\mathbf{q}$ and σ; $a_{q\sigma} = \eta_{q\sigma} + \eta^*_{q\sigma}$
$\phi_{q\sigma}$, ϕ_q, $\phi_{k\omega}$	Spectral components of $\Phi^{(1)}$ or $P^{(1)}$ after Fourier decomposition using $\mathbf{q}$ and σ ($\mathbf{k}$ and ω)
$p_{q\sigma}$, p_q, $p_{k\omega}$	$\phi_q = \phi_{q\sigma_q}$, $p_q = p_{q\sigma_q}$ where σ_q is computed from the dispersion relation
$p_{\pm}$, $\phi_{\pm}$, $\xi_{\pm}$	Second-order spectral component at a realization $\mathbf{k}_{\pm} = \mathbf{q}_1 \pm \mathbf{q}_2$ and $\omega_{\pm} = \vert\sigma_1 \pm \sigma_2\vert$
$\tilde{p}_q$, $\tilde{\phi}_q$	As p_q, ϕ_q but space-time dependence of $e^{i(\mathbf{q}^T\mathbf{x} - \sigma t)}$ are incorporated such that $P = \int\int p_q e^{i(\mathbf{q}^T\mathbf{x} - \sigma t)} d\mathbf{q} d\sigma = \int\int \tilde{p}_q d\mathbf{q} d\sigma$, and $(\tilde{p}_q, \tilde{\phi}_q)$ are real due to reflection over the q axis for $\sigma < 0$

interaction with a minimum of algebra and without the complexity of acoustic modes or bottom interactions. It is demonstrated that pressure fluctuations are produced in the water column in both microseism- and hum-frequency bands. This model demonstrates conceptually how ocean wave interactions generate microseisms and hum from sum and difference interactions. In later sections this model will be expanded to include compressibility. The notation used is given in Table 1.

2.1. Second-Order Sum and Difference Interactions

Ocean surface waves are governed by nonlinear equations and are usually solved with a perturbation expansion [*Hasselmann*, 1962; *Svendsen*, 2006]. The first-order solutions are well known and readily tractable and in many cases sufficiently describe the observable features of ocean waves. The second-order equations of motion contain terms that are quadratic in the first-order solutions. These quadratic terms act as *source terms* which force second-order pressure fluctuations that oscillate at the source term frequency. We consider a simple example with two first-order spectral components $a_1 \sin(\mathbf{q}_1^T\mathbf{x} - \sigma_1 t)$ and $a_2 \sin(\mathbf{q}_2^T\mathbf{x} - \sigma_2 t)$, with amplitude a_j, wave vector $\mathbf{q}_j$ and angular frequency σ_j, for $j \in \{1, 2\}$. These first-order waves interact to produce second-order source terms (and thus spectral components) of the form

$$S = a_1 a_2 \sin\left(\mathbf{q}_1^{\mathsf{T}}\mathbf{x} - \sigma_1 t\right) \sin\left(\mathbf{q}_2^{\mathsf{T}}\mathbf{x} - \sigma_2 t\right) = \frac{a_1 a_2}{2} \cdot \left(\sin\left[(\mathbf{q}_1 + \mathbf{q}_2)^{\mathsf{T}}\mathbf{x} - \left(\sigma_1 + \sigma_2\right) t\right] - \sin\left[(\mathbf{q}_1 - \mathbf{q}_2)^{\mathsf{T}}\mathbf{x} - (\sigma_1 - \sigma_2) t\right]\right) = p_+ + p_- \,, \tag{1}$$

where the product-to-sum trigonometric identity has been used. The two terms have wave vectors and frequencies of the sum and of the difference of the wave vectors and frequencies of the first-order waves. Note that, while the ocean surface waves are superposed, the second-order source terms are given by the first-order waves multiplied together. Thus, the second-order waves depend on the square of the first-order waves (see line 2 in equation (5)).

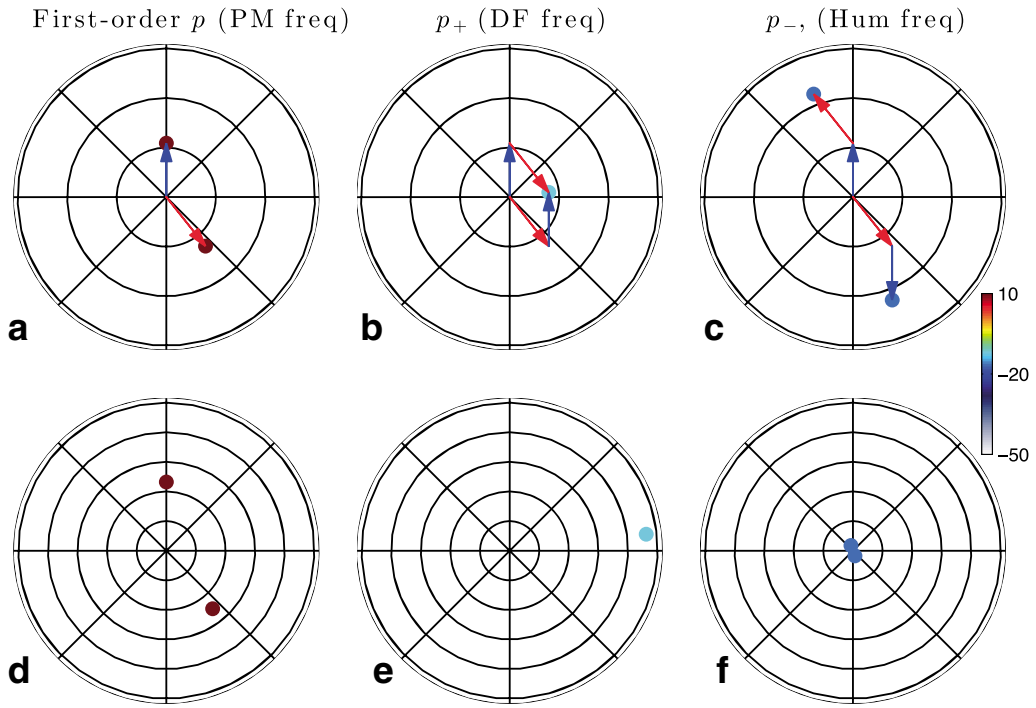

Figure 1. Two-dimensional spectra for (a) the first-order pressure p from two δ function surface waves with wave vectors $|\mathbf{q}_1| = 0.06$ and $|\mathbf{q}_1| = 0.05\ \mathrm{m}^{-1}$ and azimuths 0 and 110°), and the second-order (b) sum and (c) difference pressure $p_\pm$ with wave numbers of $\mathbf{k}_+ = \mathbf{q}_1 + \mathbf{q}_2$ and $\mathbf{k}_- = \mathbf{q}_1 - \mathbf{q}_2$ (radial rings: 0.05, 0.1, and 0.15 m^{-1}). The components are shown in (d–f) frequency-azimuth space, where the azimuth corresponds to the wave vector, and the first-order frequency in Figure 1d is σ_1, σ_2 (computed with the deepwater dispersion relation, equation (10)) and second-order frequencies are $\omega_+ = \sigma_1 + \sigma_2$ for the sum (Figure 1e) and $\omega_+ = |\sigma_1 - \sigma_2|$ for the difference (Figure 1f) pressures. (radial rings: 0.05, 0.1, 0.15, 0.2, 0.25, and 0.3 Hz). The second-order pressure amplitudes (dB referenced to kPa/Hz) computed with equation (30).

These second-order sum interactions decay exponentially with depth as $e^{-|\mathbf{q}_1+\mathbf{q}_2|z}$ and, hence, only when $\mathbf{q}_1 = -\mathbf{q}_2$, in which a depth-independent standing wave is generated, have they been considered to be important for DF microseism generation. The second-order terms for other values of $\mathbf{q}_1$ and $\mathbf{q}_2$ have been neglected in most prior work, as have the difference interactions (*Kibblewhite and Wu* [1996] is a notable exception).

We compute the full spectrum of the second-order pressure by computing a 6-D integral over the entire space defined by the frequency and 2-D wave vector for both first-order wavefields, not just the region of standing waves $\mathbf{q}_1 = -\mathbf{q}_2$. For a given first-order surface wave spectrum, the second-order spectrum contains two peaks. One at the frequency of DF microseisms p_+, forced by the *sum* term of equation (1) and one at the frequency of the Earth's seismic hum p_-, forced by the *difference* term of equation (1). The second-order pressure at hum frequencies decays exponentially with depth, whereas the second-order pressure at DF frequencies does not, consistent with the observed energy difference in DF and hum observations in the crust.

2.2. Interaction of Two Ocean Waves

The interaction of two ocean wave components is represented by δ functions in a 2-D spectrum (Figure 1a). The magnitude and direction of the second-order wave vectors depend on the relative angles of the first-order wave vectors. The sum interaction propagates at an azimuth intermediate to the azimuths of the first-order terms (Figure 1b). The difference interaction propagates in two opposing directions (Figure 1c). The frequency of the difference component is smaller than the sum component (Figures 1d–1f).

When the first-order wave energy is spread over a range of azimuths, as is common in the ocean, each component produces nonzero self interactions as well as interactions with other wave components (Figure 2). The frequency of the difference interaction is $\omega = |\sigma_1 - \sigma_2|$ and, hence, given a single wave train with energy spread over a small range of frequencies, interactions are produced at low frequencies (Figure 2f).

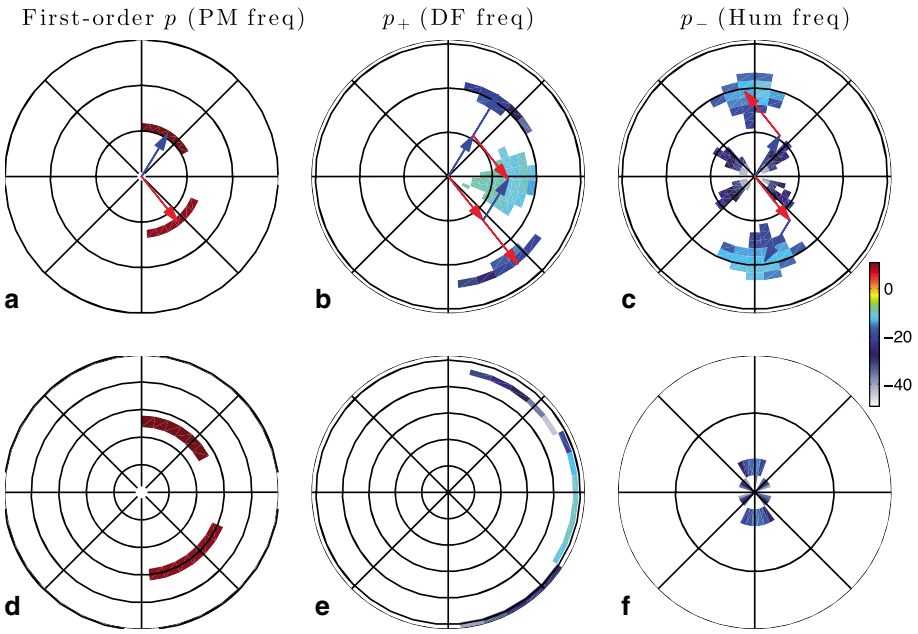

Figure 2. (a–f) Two-dimensional spectra, as for Figure 1 with two first-order surface waves with wave numbers of 0.06 and 0.05 m^{-1} and nonzero angular spread, incident at azimuths of 0–30 and 110–140°. In Figure 2f the radial axis has been magnified to reveal the very low frequency pressure components generated by difference interactions (radial rings at 0.01 and 0.02Hz).

3. Incompressible Ocean

3.1. Equations of Motion

We first expand the nonlinear surface waves to second order using the velocity potential $\Phi(\mathbf{x}, t)$ as the central variable, where the velocity is given by $\mathbf{v} = \nabla\Phi(\mathbf{x}, t)$. The vector $\mathbf{x} = (x, y, z)$ denotes horizontal (x, y) and vertical (z) displacement. Derivations of the same physical quantities can also be derived by equations in pressure [*Kibblewhite and Wu*, 1996]. Given an incompressible fluid of depth H over a rigid half-space, the dynamics are described by the conservation of mass and the boundary conditions (dynamic and kinematic) at the ocean surface and the seabed [*Hasselmann*, 1962]. This yields

$$\begin{aligned} \nabla^2\Phi &= 0 \\ \left[\frac{\partial^2}{\partial t^2} - g\frac{\partial}{\partial z}\right]\Phi &= 0 \\ \frac{\partial}{\partial t}\zeta - \frac{\partial}{\partial z}\Phi + \nabla\Phi^T\nabla\zeta &= 0 \end{aligned} \quad \text{at} \quad z = \zeta$$

$$\frac{\partial}{\partial z}\Phi = 0 \quad \text{at} \quad z = H \tag{2}$$

where $\zeta(x, t)$ is the surface displacement, g the acceleration due to gravity, and $\nabla = (\partial/\partial x, \partial/\partial y, \partial/\partial z)^{\mathrm{T}}$. Solutions to equation (2) yield the velocity potential throughout the water column, Φ, as a function of the surface wave field, ζ, which is easier to measure and model [*Ardhuin et al.*, 2012]. The pressure is obtained at any depth from the Bernoulli relation [*Kibblewhite and Wu*, 1996, p. 28]

$$P = -\rho\left(\frac{\partial}{\partial t}\Phi + \frac{1}{2}(\nabla\Phi)^2 + gz\right) \tag{3}$$

Performing a perturbation expansion, we make the substitutions [*Hasselmann*, 1962; *Kibblewhite and Wu*, 1996]

$$\Phi = \Phi^{(1)} + \Phi^{(2)}, \quad \zeta = \zeta^{(1)} + \zeta^{(2)}, \quad P = P^{(1)} + P^{(2)} \tag{4}$$

where $|\Phi^{(2)}| \ll |\Phi^{(1)}|$ and likewise for ζ and P. It is well established that the first-order pressure $P^{(1)}$ generates primary microseisms (PM) in shallow water and the second-order pressure $P^{(2)}$ generates secondary microseisms (DF) at arbitrary depth.

Equation (2) is linearized by Taylor expanding the boundary conditions about $z = 0$ and equating all terms linear in $(\Phi^{(1)}, \zeta^{(1)})$ to form the first-order equations and all terms linear in $(\Phi^{(2)}, \zeta^{(2)})$ but quadratic in $(\Phi^{(1)}, \zeta^{(1)})$ to form the second-order equations. Substituting equation (4) into the linearized equations and equating terms in this manner gives

$$\begin{aligned} \nabla^2\Phi^{(1)} &= 0 \\ \left[\frac{\partial^2}{\partial t^2} - g\frac{\partial}{\partial z}\right]\Phi^{(1)} &= 0 \\ \frac{\partial}{\partial z}\Phi^{(1)} - \frac{\partial}{\partial t}\zeta^{(1)} &= 0 \end{aligned} \Bigg\} \quad \text{at } z = 0$$
$$\frac{\partial}{\partial z}\Phi^{(1)} = 0 \qquad \text{at } z = H \tag{5}$$

and a set of second-order equations

$$\nabla^2\Phi^{(2)} = 0$$
$$\left.\begin{aligned} \left[\frac{\partial^2}{\partial t^2} - g\frac{\partial}{\partial z}\right]\Phi^{(2)} &= -\frac{\partial}{\partial t}\left(\nabla\Phi^{(1)}\right)^2 \\ \frac{\partial}{\partial z}\Phi^{(2)} - \frac{\partial}{\partial t}\zeta^{(2)} &= \nabla^T\Phi^{(1)}\nabla\zeta^{(1)} + \zeta^{(1)}\frac{\partial^2\Phi^{(1)}}{\partial z^2} \end{aligned}\right\} \quad \text{at } z=0$$
$$\frac{\partial}{\partial z}\Phi^{(2)} = 0 \qquad \text{at } z=H \tag{6}$$

The surface boundary conditions are now defined at $z = 0$ rather than $z = \zeta$. In both cases the bottom surface condition is $\frac{\partial}{\partial z}\Phi^{(1,2)} = 0$. The second-order equations are linear with respect to the second-order terms $(\Phi^{(2)}, \zeta^{(2)})$, but the forcing-terms on the right-hand side (RHS) are quadratic in the first-order terms $(\Phi^{(1)}, \zeta^{(1)})$. The RHS of the second line of equation (6) has the general form outlined in equation (1). The third line of equation (6) is not required to compute water column pressure fluctuations and is not considered further. The first- and second-order pressure are similarly derived by substituting equation (4) into equation (3),

$$\begin{aligned} P^{(1)} &= -\rho\frac{\partial}{\partial t}\Phi^{(1)} \\ P^{(2)} &= -\rho\left[\frac{\partial}{\partial t}\Phi^{(2)} + \frac{1}{2}\left(\nabla\Phi^{(1)}\right)^2\right] \end{aligned} \tag{7}$$

where the static pressure term, $-\rho gz$, is neglected as only the dynamic pressure at the seabed excites seismic waves.

We derive $\Phi^{(1,2)}$ given an arbitrary first-order surface wave $\zeta^{(1)}$ displacement spectrum. As equations (5) and (6) are linear, they must be satisfied for each frequency component. Fourier decomposition in space and time yields

$$\begin{aligned} \begin{bmatrix} \zeta^{(1)} \\ \Phi^{(1)} \\ P^{(1)} \end{bmatrix} &= \int_{-\infty}^{\infty}\int_{-\infty}^{\infty}\int_{-\infty}^{\infty}\begin{bmatrix} \eta_{\mathbf{q}\sigma} \\ \phi_{\mathbf{q}\sigma} \\ p_{\mathbf{q}\sigma} \end{bmatrix} e^{\imath(q^T\mathbf{x}-\sigma t)}\mathrm{d}\mathbf{q}\mathrm{d}\sigma \\ \begin{bmatrix} \Phi^{(2)} \\ P^{(2)} \end{bmatrix} &= \int_{-\infty}^{\infty}\int_{-\infty}^{\infty}\int_{-\infty}^{\infty}\begin{bmatrix} \phi_{\mathbf{k}\omega} \\ p_{\mathbf{k}\omega} \end{bmatrix} e^{\imath(\mathbf{k}^T\mathbf{x}-\omega t)}\mathrm{d}\mathbf{k}\mathrm{d}\omega \end{aligned} \tag{8}$$

where $\mathbf{q} = (q_x, q_y)^{\mathrm{T}}$ and σ are the wave vector and frequency of the first-order terms, and $\mathbf{k} = (k_x, k_y)^{\mathrm{T}}$ and ω are the wave vector and frequency of the second-order terms. We use different notations for the first order and second order as there is not a one-to-one correspondence between the spectral components. The subscripts $(\ldots)_{\mathbf{q}\sigma}$ and $(\ldots)_{\mathbf{k}\omega}$ differentiate the first- and second-order components.

3.2. First-Order Pressure Spectrum

Substituting equation (8) into equation (5) and Fourier transforming both sides of the equations gives

$$\begin{aligned} \left[-|\mathbf{q}|^2 + \frac{\partial^2}{\partial z^2}\right]\phi_{\mathbf{q}\sigma} &= 0 \\ \left[-\sigma^2 - g\frac{\partial}{\partial z}\right]\phi_{\mathbf{q}\sigma} &= 0 \\ \frac{\partial}{\partial z}\phi_{\mathbf{q}\sigma} + \imath\sigma\eta_{\mathbf{q}\sigma} &= 0 \end{aligned} \Bigg\} \quad \text{at } z = 0$$
$$\frac{\partial}{\partial z}\phi_{\mathbf{q}\sigma} = 0 \qquad \text{at } z = H \tag{9}$$

It is shown by substitution [*Longuet-Higgins*, 1950; *Kibblewhite and Wu*, 1996; *Svendsen*, 2006] that equation (9) is satisfied by

$$\begin{aligned}\phi_{\mathbf{q}\sigma} &= -\imath\frac{\sigma_\mathbf{q}}{|\mathbf{q}|}Z_\mathbf{q}\eta_{\mathbf{q}\sigma}\\ Z_\mathbf{q} &= \frac{\cosh(|\mathbf{q}|(H-z))}{\sinh(|\mathbf{q}|H)}\\ \sigma_\mathbf{q}^2 &= -g\frac{\partial Z_\mathbf{q}/\partial z\big|_{z=0}}{Z_\mathbf{q}(z=0)} = -g\frac{Z'_\mathbf{q}}{Z^0_\mathbf{q}} = g|\mathbf{q}|\tanh(|\mathbf{q}|H)\end{aligned} \tag{10}$$

where $Z_\mathbf{q}$ describes the depth dependence, the third equation is the standard dispersion relation for shallow-water gravity waves, and we have defined

$$Z^0_\mathbf{q} \equiv Z_\mathbf{q}(z=0) = 1/\tanh(|\mathbf{q}|H) \quad , \quad Z'_\mathbf{q} \equiv \left.\frac{\partial Z_\mathbf{q}}{\partial z}\right|_{z=0} = -|\mathbf{q}| \tag{11}$$

as the depth dependence and its derivative evaluated at $z = 0$. The dispersion relation implies $\sigma = \pm\sigma_\mathbf{q}$ and hence the integral over σ (equation (8)) can be performed as follows:

$$\begin{aligned}\int \phi_{\mathbf{q}\sigma}e^{\imath(\mathbf{q}^T\mathbf{x}-\sigma t)}\delta(\sigma\pm\sigma_\mathbf{q})\,\mathrm{d}\sigma &= -\imath\frac{\sigma_\mathbf{q}}{|\mathbf{q}|}Z_\mathbf{q}\times\left(\eta_{q,\sigma_\mathbf{q}}e^{\imath(\mathbf{q}^T\mathbf{x}-\sigma_\mathbf{q}t)}+\eta_{\mathbf{q},-\sigma_\mathbf{q}}e^{\imath(\mathbf{q}^T\mathbf{x}+\sigma_\mathbf{q}t)}\right)\\ \tilde{\phi}_\mathbf{q} &= -\imath\frac{\sigma_\mathbf{q}}{|\mathbf{q}|}Z_\mathbf{q}\left(\eta_\mathbf{q}e^{\imath\xi_\mathbf{q}}-\eta^*_\mathbf{q}e^{-\imath\xi_\mathbf{q}}\right)\\ &= -\imath\frac{\sigma_\mathbf{q}}{|\mathbf{q}|}Z_\mathbf{q}a_\mathbf{q}\sin(\xi_\mathbf{q}+\vartheta_\mathbf{q}) = \imath\frac{\sigma_\mathbf{q}}{|\mathbf{q}|}Z_\mathbf{q}a_\mathbf{q}\sin(\xi_\mathbf{q})\\ \eta_\mathbf{q} &= \eta_{\mathbf{q},\sigma_\mathbf{q}} = \eta^*_{-\mathbf{q},-\sigma_\mathbf{q}}\\ \xi_\mathbf{q} &= \mathbf{q}^T\mathbf{x}-\sigma_\mathbf{q}t \qquad a_\mathbf{q} = |\eta_\mathbf{q}|/2\end{aligned} \tag{12}$$

where the subscript σ has been dropped on the left-hand side (LHS) to signify that there is no explicit dependence of σ and the $\sim$ signifies that the second term in the RHS of equation (12) has been reflected over the $\{q_x, q_y\}$ plane (this reflection is applied to all regions of $\sigma<0$ in the $\{q_x, q_y, \sigma\}$ space). This simplifies the algebra and gives a real-valued term on the RHS but does not change the physics as the full integration still yields the same answer

$$\Phi^{(1)} = \int\tilde{\phi}_\mathbf{q}\,\mathrm{d}\mathbf{q} = \int\phi_\mathbf{q}e^{\imath(\mathbf{q}^T\mathbf{x}-\sigma_\mathbf{q}t)}\,\mathrm{d}\mathbf{q} \tag{13}$$

We split the complex-valued spectral component $\eta_\mathbf{q}$ into real-valued amplitude $a_\mathbf{q}$ and phase $\phi_\mathbf{q}$. As we are considering arbitrary surface wave power spectra, the phase is arbitrary and we assume $\vartheta_\mathbf{q} = \pi$ to eliminate a minus sign. Equation (12) is a well-known result for first-order surface waves [*Svendsen*, 2006, chapter 3].

Substituting equations (8) and (12) into equation (7) gives the first-order pressure

$$\tilde{p}_\mathbf{q} = \imath\rho\sigma_\mathbf{q}\tilde{\phi}_\mathbf{q} = \frac{\rho\sigma_\mathbf{q}^2}{|\mathbf{q}|}Z_\mathbf{q}a_\mathbf{q}\sin(\xi_\mathbf{q}) \tag{14}$$

where, similar to equation (13)

$$P^{(1)} = \int\tilde{p}_\mathbf{q}\,\mathrm{d}\mathbf{q} = \int p_\mathbf{q}e^{\imath\xi_q}\,\mathrm{d}\mathbf{q} \tag{15}$$

The notation $\tilde{}$ signifies a real-valued spectra defined by a sinusoidal Fourier transform. All other spectral terms are complex and must be Fourier transformed with a complex exponential. The former notation is easier to relate to physical quantities and prior derivations, while the second notation allows the equations to be written compactly. As expected, the first-order pressure decays hyperbolically with depth, and each spectral component p_q has a one-to-one mapping with the components of the surface wave spectra, $a_\mathbf{q}$ ($\eta_\mathbf{q}$) in the real-valued (complex) spectrum.

3.3. Second-Order Pressure Spectrum

The boundary condition of the second-order equation of motion (equation (6), we consider only the second line, as the third line only serves to define $\zeta^{(2)}$ which is not important here) is an inhomogeneous differential equation, and its solution must therefore be the sum of a homogeneous and an inhomogeneous solution. The homogeneous solution, however, is equivalent to the first-order solution [equation (10)] as the homogenous equation is identical to the first-order equation (equation (5)). The homogeneous solution will thus display the same characteristics as the first-order term, however, it is by definition much smaller than the first-order solution and is neglected.

Substituting equation (8) into the first equation in equation (6) and Fourier transforming gives

$$\left[\mathbf{k}^2 - \frac{\partial^2}{\partial z^2}\right] \phi_{\mathbf{k}\omega} = 0 \tag{16}$$

which is satisfied by a separation of variables to define a depth dependance $Z_{\mathbf{k}}$ and a surface spectrum $\varphi_{\mathbf{k}}$, where

$$\begin{aligned} \phi_{\mathbf{k},\omega} &= Z_{\mathbf{k}}(z)\varphi_{\mathbf{k}\omega} \\ Z_{\mathbf{k}} &= (C_{\mathbf{k}+}e^{|\mathbf{k}|z} + C_{\mathbf{k}-}e^{-|\mathbf{k}|z}) \end{aligned} \tag{17}$$

Substituting equation (17) into the fourth line of equation (6) with $Z_{\mathbf{k}}(z = 0) = 1$ gives the depth dependance

$$Z_{\mathbf{k}} = \frac{\cosh(|\mathbf{k}|(H-z))}{\cosh(|\mathbf{k}|H)}, \tag{18}$$

The second line in equation (6) is complicated because the two sides are being integrated over different variables. The LHS is integrated over the second-order variables $\mathbf{k}$ and ω and the RHS over the first-order wave vector $\mathbf{q}$. The following steps evaluate the RHS of equation (6) (second equation) at $z = 0$: First,

$$\begin{aligned} \nabla\Phi^{(1)} &= \int \nabla\tilde{\phi}_{\mathbf{q}}\mathrm{d}\mathbf{q} = \int \begin{bmatrix} \imath q_x Z_{\mathbf{q}} \\ \imath q_y Z_{\mathbf{q}} \\ \frac{\partial Z_{\mathbf{q}}}{\partial z} \end{bmatrix}_{z=0} \tilde{\varphi}_{\mathbf{q}}\,\mathrm{d}\mathbf{q} \\ &= \int \begin{bmatrix} \imath q_x Z^0_{\mathbf{q}} \\ \imath q_y Z^0_{\mathbf{q}} \\ Z'_{\mathbf{q}} \end{bmatrix} \frac{\sigma_{\mathbf{q}}}{|\mathbf{q}|}\left(\eta_{\mathbf{q}}e^{\imath\xi_{\mathbf{q}}} + \eta^*_{\mathbf{q}}e^{-\imath\xi_{\mathbf{q}}}\right)\mathrm{d}\mathbf{q} \end{aligned} \tag{19}$$

which follows from equations (10)–(13), and where $\varphi_{\mathbf{q}}$ is the first-order spectrum separated from the depth-dependance. Second,

$$\begin{aligned} \left(\nabla\Phi^{(1)}\right)^2 &= \nabla^{\mathrm{T}}\Phi^{(1)}(\mathbf{q}_1)\nabla\Phi^{(1)}(\mathbf{q}_2) \\ &= \int\int \left(Z'_1Z'_2 - Z^0_1Z^0_2\mathbf{q}_1^T\mathbf{q}_2\right)\frac{\sigma_1\sigma_2}{\mathbf{q}_1\mathbf{q}_2}\left(\eta_1\eta_2e^{\imath(\xi_1+\xi_2)}\right. \\ &\quad \left.+\eta_1\eta^*_2e^{\imath(\xi_1-\xi_2)} + \eta^*_1\eta_2e^{\imath(\xi_2-\xi_1)} + \eta^*_1\eta^*_2e^{-\imath(\xi_1+\xi_2)}\right)\mathrm{d}\mathbf{q}_1\mathrm{d}\mathbf{q}_2 \\ &= \iint\Theta\left[|\eta_1\eta_2|\cos(\xi_1+\xi_2) + |\eta^*_1\eta_2|\cos(\xi_2-\xi_1)\right]\mathrm{d}\mathbf{q}_1\mathrm{d}\mathbf{q}_2 \end{aligned} \tag{20}$$

where we used the notation $\sigma_{\mathbf{q}_j} = \sigma_j$, $\eta_{\mathbf{q}_j} = \eta_j$, and $\xi_{\mathbf{q}_j} = \xi_j$. We have utilized the independence of the integration variables $\mathbf{q}_1$ and $\mathbf{q}_2$ and, once again, we have incorporated the phase terms into $\xi_j = \xi_j + \vartheta_{\mathbf{q}_j}$. The factor Θ is given by

$$\begin{aligned} \Theta &= 2\frac{\sigma_1\sigma_2}{\mathbf{q}_1\mathbf{q}_2}\left(Z'_1Z'_2 - Z^0_1Z^0_2\mathbf{q}_1^T\mathbf{q}_2\right) \\ &= 2\frac{\sigma_1\sigma_2}{\mathbf{q}_1\mathbf{q}_2}\left(Z'_1Z'_2 - Z^0_1Z^0_2|\mathbf{q}_1\mathbf{q}_2|\cos\theta_{12}\right) \end{aligned} \tag{21}$$

which introduces a multiplicative scaling on the amplitude of the second-order waves. This varies with the relative angle θ_{12} between the direction of propagation of the two first-order spectral components from

which the second-order spectral component is forced. Opposing components produce the largest amplitude interactions. In deep water, $Z^0_{\mathbf{q}} \to 1$ and, as $Z'_{\mathbf{q}} = -|\mathbf{q}|$, the RHS of equation (21) is zero when $\theta_{12} = 0$. Thus, deepwater waves propagating in parallel produce no second-order forcing.

Performing the time derivative gives the RHS of the second equation in equation (6)

$$-\frac{\partial}{\partial t}\left(\nabla\Phi^{(1)}\right)^2 = \int\int \Theta\left[(\sigma_1+\sigma_2)|\eta_1\eta_2|\sin(\xi_1+\xi_2) + (\sigma_2-\sigma_1)|\eta_1^*\eta_2|\sin(\xi_2-\xi_1)\right] \mathrm{d}\mathbf{q}_1\mathrm{d}\mathbf{q}_2 \tag{22}$$

Substituting equation (22) into the RHS and equation (8) into the LHS of equation (6) gives

$$\int\int \left[-\omega^2 + g|\mathbf{k}|\tanh(|\mathbf{k}|H)\right]\phi_{k\omega}e^{i\xi_{\mathbf{k}\omega}}\,\mathrm{d}\mathbf{k}\mathrm{d}\omega = \int\int \Theta\left[(\sigma_1+\sigma_2)|\eta_1\eta_2|\sin(\xi_1+\xi_2) + (\sigma_2-\sigma_1)|\eta_1^*\eta_2|\sin(\xi_2-\xi_1)\right] \mathrm{d}\mathbf{q}_1\mathrm{d}\mathbf{q}_2 \tag{23}$$

Fourier transforming, $\int\int \ldots e^{-\imath(\mathbf{k}^T\mathbf{x}-\omega t)}\mathrm{d}\mathbf{x}\mathrm{d}t$ equation (23) gives

$$\phi_{\mathbf{k}\omega}(z=0) = \frac{\omega}{D}\left[S_+(\mathbf{k},\omega) + S_-(\mathbf{k},\omega)\right] \tag{24}$$

where the ω on the RHS stems from the $\sigma_2+\sigma_1$ and $\sigma_2-\sigma_1$ in equation (23) which have been taken outside the integral, and

$$\begin{aligned} D(\mathbf{k},\omega) &= -\omega^2 Z^0_{\mathbf{k}} - gZ'_{\mathbf{k}} = g|\mathbf{k}|\tanh(|\mathbf{k}|H) - \omega^2 \\ S_+(\mathbf{k},\omega) &= \int\int \frac{\Theta}{2}|\eta_1\eta_2|\left[\delta(\mathbf{k}-(\mathbf{q}_1+\mathbf{q}_2))\delta(\omega-(\sigma_1+\sigma_2)) - \delta(\mathbf{k}+(\mathbf{q}_1+\mathbf{q}_2))\delta(\omega+(\sigma_1+\sigma_2))\right]\mathrm{d}\mathbf{q}_1\mathrm{d}\mathbf{q}_2 \\ S_-(\mathbf{k},\omega) &= \iint \frac{\Theta}{2}|\eta_1^*\eta_2|\left[\delta(\mathbf{k}-(\mathbf{q}_1-\mathbf{q}_2))\delta(\omega-(\sigma_1-\sigma_2)) - \delta(\mathbf{k}+(\mathbf{q}_1-\mathbf{q}_2))\delta(\omega+(\sigma_1-\sigma_2))\right]\mathrm{d}\mathbf{q}_1\mathrm{d}\mathbf{q}_2 \end{aligned} \tag{25}$$

where we have used $\int\int \sin(\mathbf{k}'^T\mathbf{x}-\omega' t)e^{\imath(\mathbf{k}'^T\mathbf{x}-\omega t)}\mathrm{d}\mathbf{x}\mathrm{d}t = 1/2\left[\delta(\mathbf{k}-\mathbf{k}')\delta(\omega-\omega') - \delta(\mathbf{k}+\mathbf{k}')\delta(\omega+\omega')\right]$. Due to the sifting properties of the δ functions, the integrals in equation (25) reduce to the sum of two points in the $\{\mathbf{q}_1,\mathbf{q}_2\}$ space for each $\mathbf{k}$ and ω (Figures 4a and 4b). We have also used $Z^0_{\mathbf{k}} = Z_{\mathbf{k}}(z=0)$ and $Z'_{\mathbf{k}} = \partial Z_{\mathbf{k}}/\partial z\big|_{z=0}$ as in the first order.

Introducing the variables

$$\mathbf{k}_+ = \mathbf{q}_1 + \mathbf{q}_2\,, \quad \omega_+ = \sigma_1+\sigma_2 \tag{26}$$

$$\mathbf{k}_- = \mathbf{q}_1 - \mathbf{q}_2\,, \quad \omega_- = \sigma_1-\sigma_2 \tag{27}$$

which represent the sum and difference component of the interacting first-order waves. This simplifies the integrals in equation (25)

$$\begin{aligned} S_+(\mathbf{k},\omega) &= \int\int \frac{\Theta}{2}|\eta_1\eta_2|\left[\delta(\mathbf{k}-\mathbf{k}_+)\delta(\omega-\omega_+) - \delta(\mathbf{k}+\mathbf{k}_+)\delta(\omega+\omega_+)\right]\mathrm{d}\mathbf{q}_1\mathrm{d}\mathbf{q}_2 \\ S_-(\mathbf{k},\omega) &= \int\int \frac{\Theta}{2}|\eta_1^*\eta_2|\left[\delta(\mathbf{k}-\mathbf{k}_-)\delta(\omega-\omega_-) - \delta(\mathbf{k}+\mathbf{k}_-)\delta(\omega+\omega_-)\right]\mathrm{d}\mathbf{q}_1\mathrm{d}\mathbf{q}_2 \end{aligned} \tag{28}$$

The integration contours defined by the δ functions in $\{\mathbf{q}_1,\mathbf{q}_2\}$ space for two opposing waves are shown in Figures 4a and 4b. Note that the variables $\eta_1, \eta_2, \Theta, \mathbf{k}_\pm$, and $\omega_\pm$ depend on $\mathbf{q}_1$ and $\mathbf{q}_2$ (Figures 4c and 4d) and thus are important in the integration. We refer to these terms as the *sum* S_+ and *difference* S_- interactions. Given two opposing narrowband waves such that $|\eta_{\mathbf{q}}|$ is peaked around $\mathbf{q}_1$ and $\mathbf{q}_2$, the sum interactions peak around wave vectors of $\mathbf{k}_+ = \mathbf{q}_1 + \mathbf{q}_2$ and frequencies around $\omega_+ = \sigma_1+\sigma_2$, and the difference interactions peak around $\mathbf{k}_- = \mathbf{q}_1 - \mathbf{q}_2$ and $\omega_- = \sigma_1 - \sigma_2$.

Combining equations (24) with (18) gives the second-order amplitude spectrum

$$\phi_{\mathbf{k}\omega} = \frac{Z_{\mathbf{k}}}{D}\omega\left[S_+(\mathbf{k},\omega) + S_-(\mathbf{k},\omega)\right] \tag{29}$$

Equation (29) is infinite if $\omega^2 = g|\mathbf{k}|\tanh(|\mathbf{k}|H)$ but substituting, $\mathbf{k} = \mathbf{q}_1 \pm \mathbf{q}_2$, $\omega = |\sigma_1 \pm \sigma_2|$ and $\sigma_j^2 = g|\mathbf{q}_j|\tanh(|\mathbf{q}_j|H)$ shows that equality only occurs in the trivial case where $\sigma_1 = 0$ or $\sigma_2 = 0$, and therefore, $S_{k\omega} = 0$ [*Hasselmann*, 1962]. Equation (29) therefore remains finite for all ω and $\mathbf{k}$.

Substituting equations (29) and (10) into equation (7) gives the second-order pressure

$$\begin{aligned} p_{\mathbf{k}\omega} &= \frac{-\rho\omega^2 Z}{D}\left[S_+(\mathbf{k},\omega) + S_-(\mathbf{k},\omega)\right] - \frac{\rho}{2}\left[\check{S}_+(\mathbf{k},\omega) + \check{S}_-(\mathbf{k},\omega)\right] \\ &= p_+ + p_- \end{aligned} \tag{30}$$

where

$$\begin{aligned} p_\pm &= -\frac{\rho\omega^2 Z}{D}S_\pm(\mathbf{k},\omega) - \frac{\rho}{2}\check{S}_\pm(\mathbf{k},\omega) \\ \check{S}_\pm(k,\omega) &= \int\int \check{Z}\frac{\Theta}{2}|\eta_1\eta_2|\delta\left(\mathbf{k}-\mathbf{k}_\pm\right)\delta\left(\omega-\omega_\pm\right)\mathrm{d}\mathbf{q}_1\mathrm{d}\mathbf{q}_2 \\ \check{Z} &= Z_{\mathbf{q}1}Z_{\mathbf{q}2} = \frac{\cosh\left[|\mathbf{q}_1|(H-z)\right]}{\cosh\left(\left[|\mathbf{q}_1|H\right)\right.}\frac{\cosh\left[|\mathbf{q}_2|(H-z)\right]}{\cosh\left(\left[|\mathbf{q}_2|H\right)\right.} \end{aligned} \tag{31}$$

The first term in $p_\pm$ is due to the second-order velocity potential, and the second term is due to the quadratic first-order term in equation (7). The $\check{S}_\pm$ terms decay rapidly away from the surface and have been neglected in most prior work (*Kibblewhite and Wu* [1996] is a notable exception). $\check{S}_\pm$ differs from $S_\pm$ in depth dependence which, in equation (31), is inside the integral. The S_+ terms do not decay with depth when $\mathbf{q}_1 = -\mathbf{q}_2$ (considered in the following section), but the $\check{S}_+$ terms nonetheless decay exponentially in this case.

To investigate the effect of the $\check{S}_\pm$ terms, which may be important in shallow water, the pressure from just these terms is also computed

$$\check{p}_\pm = \frac{\rho}{2}\check{S}_\pm(\mathbf{k},\omega) \tag{32}$$

3.4. Double-Frequency Approximation

In the case where $\mathbf{q}_1 \approx -\mathbf{q}_2$, such that

$$\begin{aligned} |\mathbf{k}| \approx 0, \quad \omega \approx 2\sigma_{\mathbf{q}} = 2\sqrt{g|\mathbf{q}|}\tanh(|\mathbf{q}|H) \\ \Theta \approx 2\sigma_{\mathbf{q}}\sigma_{\mathbf{q}}(1+1) = 4\sigma_{\mathbf{q}}^2 \\ \cos(\xi_{k\omega}) \approx \cos(2\sigma t) \\ Z_{\mathbf{k}} \approx 1, \qquad D \approx \omega^2 = 4\sigma_q^2 \end{aligned} \tag{33}$$

the rate of exponential decay with depth is negligible, and thus, these components propagate in deep water without decay. Prior works (*Kibblewhite and Wu* [1996] being a notable exception) have assumed these double-frequency (DF) terms dominant and integrated $\{q_1, q_2\}$ space over the region in which $q_1 = -q_2$ [*Longuet-Higgins*, 1950; *Hasselmann*, 1963]. This region is the diagonal, marked by $k = 0$ in the sum interaction contours (Figure 4a) and by $\omega = 0$ in the difference interaction contours (Figure 4b).

Evaluating the second-order components, only along the contour $k = 0$ is the DF approximation. The integration region κ_{DF} is given by

$$\int\int_{\kappa_{\mathrm{DF}}(\omega)} \ldots \mathrm{d}q_1\mathrm{d}q_2 = \int\int \ldots \delta(q_1-q_2)\delta(\omega-2\sigma_1)\mathrm{d}q_1\mathrm{d}q_2 \tag{34}$$

and applying these integration limits, substituting equation (33) into equation (30), and neglecting the $\check{p}_\pm$ terms, which decay exponentially, gives the DF approximation of the second-order pressure as

$$p_{\mathrm{DF}}(\sigma) = -2\rho\sigma^2 a_\sigma^2\cos(2\sigma t) \tag{35}$$

consistent with *Longuet-Higgins* [1950, equations (31) and (175)]. In deep waters, equation (30) tends to equation (35), and the first-order pressure [equation (14)] tends to zero.

4. Compressibility

Here we develop the theory for a compressible ocean. Other than the change in depth dependance, the first- and second-order pressure spectra in a compressible fluid (equations (45) and (53)) are almost identical to those of a compressible fluid (equations (14) and (30)). Thus, the second-order spectral peaks at frequencies corresponding to DF microseisms (sum contributions) and the Earth's seismic hum (difference contributions) will be present in a compressible fluid.

In a compressible ocean with acoustic wave velocity

$$c^2 = \frac{\partial p}{\partial \rho} \tag{36}$$

the boundary conditions (the later lines of equations (5) and (6) in the incompressible case) are unchanged. The linearized continuity equations (the first line of equations (5) and (6)) become [e.g., *Kibblewhite and Wu*, 1996]

$$\nabla^2 \Phi^{(1,2)} + \frac{g}{c^2}\frac{\partial}{\partial z}\Phi^{(1,2)} - \frac{1}{c^2}\frac{\partial^2}{\partial t^2}\Phi^{(1,2)} = 0 \tag{37}$$

which is strictly true for the first order and asymptotically true for the second-order equation. The full second-order equation contains a term (not shown) on the RHS of equation (37). The compressible terms on the LHS are due to surface loading (compressibility induced corrections from motions of the surface). The compressible term on the neglected RHS is due to "internal loading in the water column" (compressibility induced corrections from bulk-fluid motion). The latter contribution can be shown to be insignificant and hence is neglected [e.g., *Kibblewhite and Wu*, 1996]. The new terms in equation (37) describe how the fluid velocity is affected by density fluctuations caused by the vertical motion of the sea surface.

4.1. First-Order Pressure Spectrum

Substituting equation (8) into equation (5) and Fourier transforming both sides of the equations gives

$$\begin{aligned} \left[-|\mathbf{q}|^2 + \tfrac{\partial^2}{\partial z^2} + \tfrac{g}{c^2}\tfrac{\partial}{\partial z} + \tfrac{\sigma^2}{c^2}\right]\phi_{\mathbf{q}\sigma} &= 0 \\ \left[-\sigma^2 - g\tfrac{\partial}{\partial z}\right]\phi_{\mathbf{q}\sigma} &= 0 \\ \tfrac{\partial}{\partial z}\phi_{\mathbf{q}\sigma} - \imath\sigma\eta_{\mathbf{q}\sigma} &= 0 \end{aligned} \Bigg\} \text{ at } z = 0$$
$$\tfrac{\partial}{\partial z}\phi_{\mathbf{q}\sigma} = 0 \quad \text{at } z = H \tag{38}$$

Note that equation (38) is identical to equation (9) except for the first-line. Defining

$$\begin{aligned} K^2 &= |\mathbf{q}|^2 - \sigma_{\mathbf{q}}^2/c^2 \\ a &= g/2c^2 \\ Q_{\mathbf{q}} &= \sqrt{a^2 + K^2} = \sqrt{|\mathbf{q}|^2 + (g^2/4c^2 - \sigma_{\mathbf{q}}^2)/c^2} \\ \Gamma_{\pm} &= -a \pm Q_{\mathbf{q}} = -\frac{g}{2c^2} \pm \sqrt{|\mathbf{q}|^2 + (g^2/4c^2 - \sigma_{\mathbf{q}}^2)/c^2} \end{aligned} \tag{39}$$

The first-order solutions to the compressible equations of equation (38) is

$$\phi_{\mathbf{q}\sigma} = -\imath\frac{\sigma_{\mathbf{q}}}{|\mathbf{q}|}\Xi_{\mathbf{q}}\eta_{\mathbf{q}\sigma} \tag{40}$$

$$\begin{aligned} \Xi_{\mathbf{q}} &= C_{\mathbf{q}+}e^{(-a+Q_{\mathbf{q}})z} + C_{\mathbf{q}-}e^{(-a-Q_{\mathbf{q}})z} \\ &= e^{-az}(C_{\mathbf{q}+}e^{Q_{\mathbf{q}}z} + C_{q-}e^{-Q_{\mathbf{q}}z}) \end{aligned} \tag{41}$$

$$\begin{aligned} C_{\mathbf{q}+} &= -\frac{|\mathbf{q}|e^{-Q_{\mathbf{q}}H}}{\Gamma_{\mathbf{q}+}(e^{Q_{\mathbf{q}}H} - e^{-Q_{\mathbf{q}}H})} = -\frac{|\mathbf{q}|}{\Gamma_{\mathbf{q}+}}\frac{e^{-Q_{\mathbf{q}}H}}{2\sinh(Q_{\mathbf{q}}H)} \\ C_{\mathbf{q}-} &= \frac{|\mathbf{q}|e^{Q_{\mathbf{q}}H}}{\Gamma_{\mathbf{q}-}(e^{Q_{\mathbf{q}}H} - e^{-Q_{\mathbf{q}}H})} = \frac{|\mathbf{q}|}{\Gamma_{\mathbf{q}-}}\frac{e^{+Q_{\mathbf{q}}H}}{2\sinh(Q_{\mathbf{q}}H)} \end{aligned} \tag{42}$$

$$\sigma_{\mathbf{q}}^2 = g\frac{\Xi'_{\mathbf{q}}}{\Xi^0_{\mathbf{q}}} = gK^2\frac{\sinh(Q_{\mathbf{q}}H)}{Q_{\mathbf{q}}\cosh(Q_{\mathbf{q}}H) - a\sinh(Q_{\mathbf{q}}H)} \tag{43}$$

where $\Xi_{\mathbf{q}}$ describes the depth dependence, equation (43) is the dispersion relation, and once again, we define the depth dependance and its derivative at the surface

$$\Xi^0_{\mathbf{q}} \equiv \Xi_{\mathbf{q}}(z=0) = C_{\mathbf{q}+} + C_{q-}\,,\ \Xi'_{\mathbf{q}} \equiv \left.\frac{\partial \Xi_{\mathbf{q}}}{\partial z}\right|_{z=0} = C_{\mathbf{q}+}\Gamma_{\mathbf{q}+} + C_{\mathbf{q}-}\Gamma_{\mathbf{q}-} \tag{44}$$

As in the compressible case, the dispersion relation implies $\sigma = \pm\sigma_{\mathbf{q}}$, and hence, the integral over σ (equation (8)) becomes (following equations (12)–(14))

$$\begin{aligned}\tilde{p}_{\mathbf{q}} &= \imath\rho\sigma_{\mathbf{q}}\tilde{\phi}_{\mathbf{q}} = \rho\frac{\sigma^2_{\mathbf{q}}}{|\mathbf{q}|}\Xi_{\mathbf{q}}\left(\eta_{\mathbf{q}}e^{\imath\xi_q} - \eta^*_{\mathbf{q}}e^{-\imath\xi_{\mathbf{q}}}\right)\\ &= \rho\frac{\sigma^2_{\mathbf{q}}}{|\mathbf{q}|}\Xi_{\mathbf{q}}a_{\mathbf{q}}\sin(\xi_{\mathbf{q}})\end{aligned} \tag{45}$$

Note that in the limiting case as $c \to \infty$,

$$\begin{aligned}K \to |\mathbf{q}| \quad &, \quad a \to 0 \quad , \quad Q \to |\mathbf{q}|\\ \Gamma_{\pm} \to \pm|\mathbf{q}| \quad &, \quad \Xi_{\mathbf{q}} \to Z_{\mathbf{q}} \quad , \quad \sigma^2_{\mathbf{q}} = g\frac{\Xi'_{\mathbf{q}}}{\Xi^0_{\mathbf{q}}} \to g\frac{Z'_{\mathbf{q}}}{Z^0_{\mathbf{q}}}\end{aligned} \tag{46}$$

4.2. Second-Order Pressure Spectrum

Substitution of equation (8) into the second-order continuity equation and Fourier transforming gives

$$\begin{aligned}\left[-|\mathbf{k}|^2 + \frac{\partial^2}{\partial z^2} + \frac{g}{c^2}\frac{\partial}{\partial z} + \frac{\sigma^2}{c^2}\right]\phi_{\mathbf{k}\omega} = 0\\ \frac{\partial}{\partial z}\phi_{\mathbf{k}\omega} = 0 \quad \text{at } z = H\end{aligned} \tag{47}$$

which corresponds to equation (16) in the incompressible case. Equation (47) is satisfied by

$$\begin{aligned}\phi_{\mathbf{k}\omega} &= \Xi_{\mathbf{k}}(z)\varphi(\mathbf{k},\omega)\\ \Xi_{\mathbf{k}} &= C_{\mathbf{k}+}e^{(-a+Q_{\mathbf{k}})z} + C_{\mathbf{k}-}e^{(-a-Q_{\mathbf{k}})z}\\ Q_{\mathbf{k}} &= \sqrt{\mathbf{k}^2 - \omega^2/c^2}\end{aligned} \tag{48}$$

where $\varphi(\mathbf{k},\omega)$ gives the field at the surface, and the depth dependence is given by $\Xi_{\mathbf{k}}(z)$. The constants $C_{\mathbf{k}+}, C_{\mathbf{k}-}$ are found from line 2 in equation (47) and at the surface, $\Xi_{\mathbf{k}}(z=0) = 1$:

$$\begin{aligned}C_{\mathbf{k}+} &= \frac{(a+Q)e^{-Q_{\mathbf{k}}H}}{2(Q_{\mathbf{k}}\cosh(Q_{\mathbf{k}}H) - a\sinh(Q_{\mathbf{k}}H))}\\ C_{\mathbf{k}-} &= \frac{(-a+Q)e^{Q_{\mathbf{k}}H}}{2(Q_{\mathbf{k}}\cosh(Q_{\mathbf{k}}H) - a\sinh(Q_{\mathbf{k}}H))}\end{aligned} \tag{49}$$

Note that the depth dependance is similar to the first-order but the dispersion relation no longer holds, ω and $\mathbf{k}$ vary independently.

The surface boundary condition

$$\left[\frac{\partial^2}{\partial t^2} - g\frac{\partial}{\partial z}\right]\Phi^{(2)} = -\frac{\partial}{\partial t}\left(\nabla\Phi^{(1)}\right)^2 \tag{50}$$

is identical to the incompressible case except the depth dependance terms have changed: $Z^0_{\mathbf{q}} \to \Xi^0_{\mathbf{q}}$ and $Z'_{\mathbf{q}} \to \Xi'_{\mathbf{q}}$. Thus, the following equations (19)–(29) give the compressible second-order velocity potential

$$\phi_{\mathbf{k}\omega} = \frac{\Xi_{\mathbf{k}}}{D}\omega\left[S_+(\mathbf{k},\omega) + S_-(\mathbf{k},\omega)\right] \tag{51}$$

where

$$\begin{aligned}D(\mathbf{k},\omega) &= -\omega^2\Xi^0_{\mathbf{k}} - g\Xi'_{\mathbf{k}}\\ S_+(\mathbf{k},\omega) &= \iint\frac{\Theta}{2}|\eta_1\eta_2|\left[\delta(\mathbf{k}-\mathbf{k}_+)\delta(\omega-\omega_+)\right.\\ &\quad\left.-\delta(\mathbf{k}+\mathbf{k}_+)\delta(\omega+\omega_+)\right]\mathrm{d}\mathbf{q}_1\mathrm{d}\mathbf{q}_2\\ S_-(\mathbf{k},\omega) &= \iint\frac{\Theta}{2}|\eta^*_1\eta_2|\left[\delta(\mathbf{k}-\mathbf{k}_-)\delta(\omega-\omega_-)\right.\\ &\quad\left.-\delta(\mathbf{k}+\mathbf{k}_-)\delta(\omega+\omega_-)\right]\mathrm{d}\mathbf{q}_1\mathrm{d}\mathbf{q}_2\\ \Theta &= 2\frac{\sigma_1\sigma_2}{\mathbf{q}_1\mathbf{q}_2}\left(\Xi'_1\Xi'_2 - \Xi^0_1\Xi^0_2|\mathbf{q}_1\mathbf{q}_2|\cos\theta_{12}\right)\end{aligned} \tag{52}$$

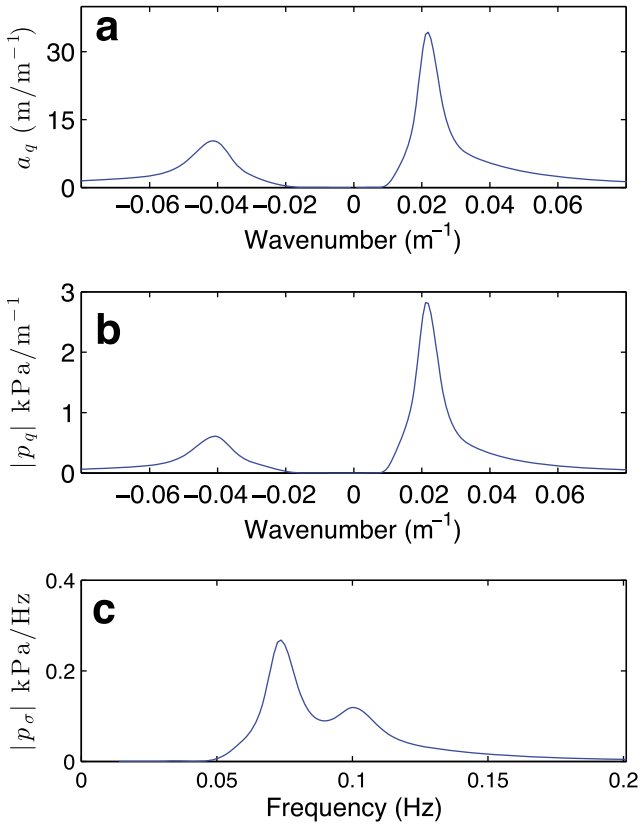

Figure 3. (a) First-order surface wave spectrum $|a_q^{(1)}|$, (equation (12)) given by the JONSWAP model and the first-order pressure $|p_q|$ at the surface (equation (14)) against (b) wave vector (q) and (c) frequency $[\sigma/(2\pi)]$.

where once again we have defined the second-order depth dependancies at the surface $\Xi_{\mathbf{k}}^0 = \Xi_{\mathbf{k}}(z=0)$ and $\Xi'_{\mathbf{k}} = \partial\Xi_{\mathbf{k}}/\partial z|_{z=0}$.

Substituting equation (52) into equation (7) gives

$$\begin{aligned} p_{\mathbf{k}\omega} &= \frac{-\rho\omega^2\Xi_{\mathbf{k}}}{D}\left[S_+(\mathbf{k},\omega)+S_-(\mathbf{k},\omega)\right] - \frac{\rho}{2}\left[\check{S}_+(\mathbf{k},\omega)+\check{S}_-(\mathbf{k},\omega)\right] \\ &= p_+ + p_- \end{aligned} \tag{53}$$

where

$$\begin{aligned} p_\pm &= -\frac{\rho\omega^2\Xi_{\mathbf{k}}}{D}S_\pm(\mathbf{k},\omega) - \frac{\rho}{2}\check{S}_\pm(\mathbf{k},\omega) \\ \check{S}_\pm(k,\omega) &= \int\int \check{\Xi}\frac{\Theta}{2}|\eta_1\eta_2|\delta(\mathbf{k}-\mathbf{k}_\pm)\delta\left(\omega-\omega_\pm\right)\mathrm{d}\mathbf{q}_1\mathrm{d}\mathbf{q}_2 \\ \check{\Xi} &= \Xi_{\mathbf{q}1}\Xi_{\mathbf{q}2} \end{aligned} \tag{54}$$

Note that the second-order pressure in a compressible fluid is identical to that of an incompressible fluid except that the multiplicative factor D and the directional dependance Θ are now defined by the compressible depth dependence, $\Xi_{\mathbf{q}}$ and $\Xi_{\mathbf{k}}$, rather than the incompressible forms $Z_{\mathbf{q}}$ and $Z_{\mathbf{k}}$. As in the incompressible solutions the rate of decay with depth varies with wave number and frequencies.

When $\Gamma_\pm$ are real, $\Xi_{\mathbf{k}}$ behaves qualitatively as Z and the pressure equation describes bulk movements of the fluid due to surface wave-motion. When $\Xi_{\mathbf{k}}$ is complex, as occurs when

$$\begin{aligned} \sigma_{\mathbf{q}}^2 &> c^2|\mathbf{q}|^2 + 1/4(g/c)^2 \\ \omega^2 &> c^2|\mathbf{k}|^2 + 1/4(g/c)^2 \end{aligned} \tag{55}$$

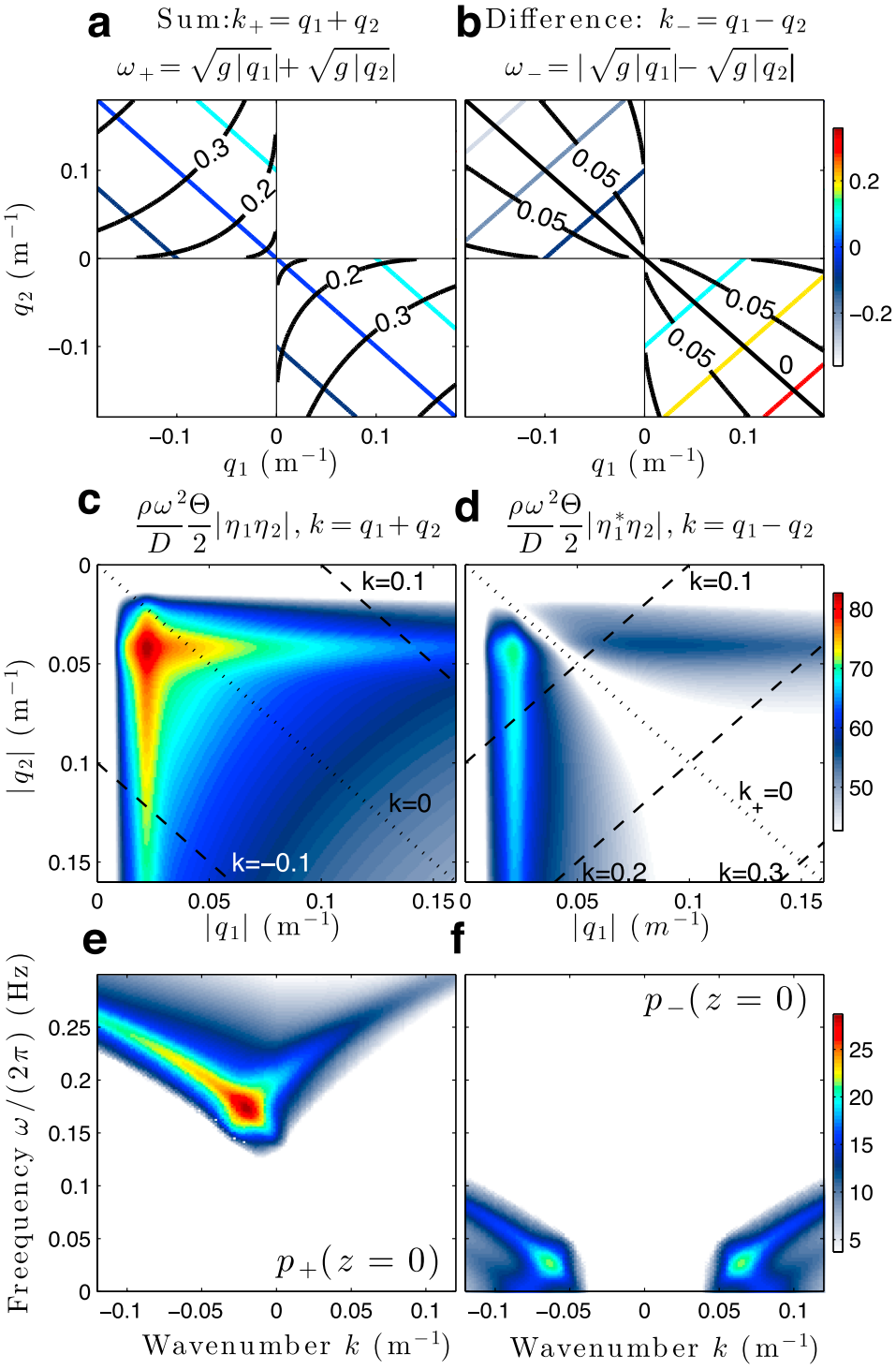

Figure 4. Contours of second-order wave number ($k_\pm = |q_1| \pm |q_2|$, color) and frequency ($\omega_\pm = \sigma_1 \pm \sigma_2$, black) against the first-order wave numbers for 1-D (a) sum and (b) difference interactions ($H = \infty$). Only the second and fourth quadrants are shown as Θ (equation (21)) is zero in the other quadrants. The integrands of equation (28) ($\Theta/2|\eta_1^{(*)}\eta_2|$) are shown for the (c) sum and (d) difference interactions over the fourth quadrant of Figures 4a and 4b multiplicated by $\rho\omega^2/D$ to give units of pressure. Contours of k are plotted in black and the $k_+ = 0$, is shown (dotted line) in both Figures 4c and 4d. The integral in equation (28) is evaluated by summing the values in Figures 4c and 4d over the contours in Figures 4a and 4b to give second-order (e) sum and (f) difference surface pressures as a function of k and ω (dB referenced to Pa/(m^{-1}Hz).

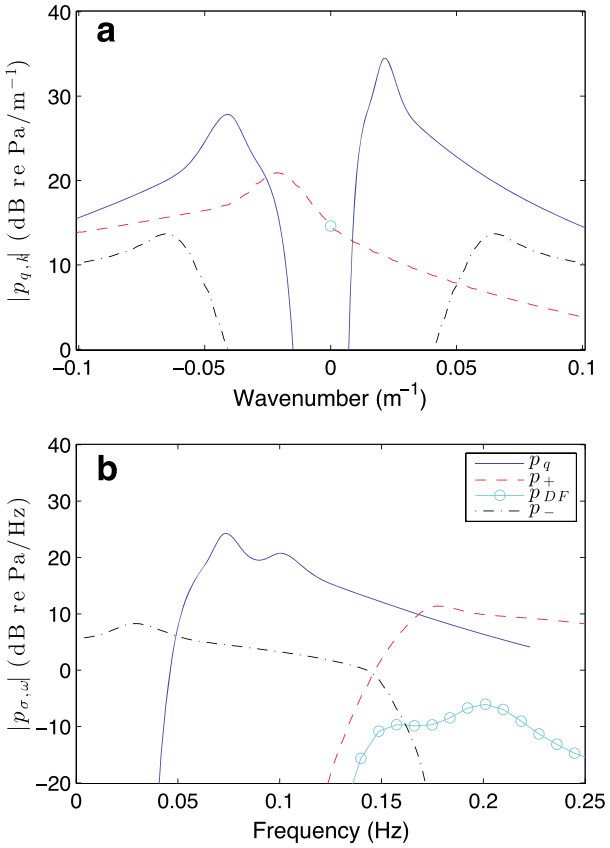

Figure 5. Pressure spectra (at the ocean surface $z = 0$) of the first-order (p_q, solid line), and second-order sum (p_+, dashed line) and difference (p_-), dashed-dotted line) components against (a) wave vector k and (b) frequency (σ or ω). The DF approximation p_{DF} (∘) is obtained by integrating over the region of $\{q_1, q_2\}$ space where $k = 0$ (the dotted line along the diagonals of Figures 4c and 4d).

for the first-order and second-order solutions, then $\Xi_{\mathbf{k}}$ becomes a complex-valued exponential. In the special case where $\mathrm{Re}(\Gamma_{\pm}) = 0$, then $|\Xi_{\mathbf{k}}|$ does not decay with depth. This describes a propagating acoustic wave. Thus, there will be certain points in the wave number-frequency plane, where surface wave energy excite propagating acoustic modes. These may excite standing waves such that certain wave numbers and frequencies resonate in the water column and thus the pressure spectrum at depth will be dominated by these discrete nodes [*Longuet-Higgins*, 1950; *Hasselmann*, 1963; *Ardhuin and Herbers*, 2013].

5. Simulations

5.1. One-Dimensional Incompressible Infinitely Deep Ocean

We numerically compute the first and second-order solutions to the incompressible equations (sections 3.2 and 3.3) with a realistic first-order surface wave spectrum. Initially, we minimize the algebra by considering only waves propagating in one dimensional such that $\theta_{12} = \{0, \pi\}$ and setting the ocean depth $H \to \infty$ such that equations (10), (18), and (21) become

$$Z_{\mathbf{q}} \to e^{-|\mathbf{q}|z} \quad , \quad \sigma_{\mathbf{q}}^2 \to g|\mathbf{q}| \quad , \quad Z_{\mathbf{k}} \to e^{-|\mathbf{k}|z}$$
$$\Theta \to \begin{cases} 0 & \theta_{12} = 0 \\ 2\sigma_{\mathbf{q}1}\sigma_{\mathbf{q}2} & \theta_{12} = \pi \end{cases} \tag{56}$$

5.1.1. Surface Wave Spectrum

The first-order surface wave spectrum a_q (equation (14)) is constructed with two opposing wavefields in a one-dimensional space. The two wavefields are generated with the Joint North Sea Wave Project (JONSWAP)

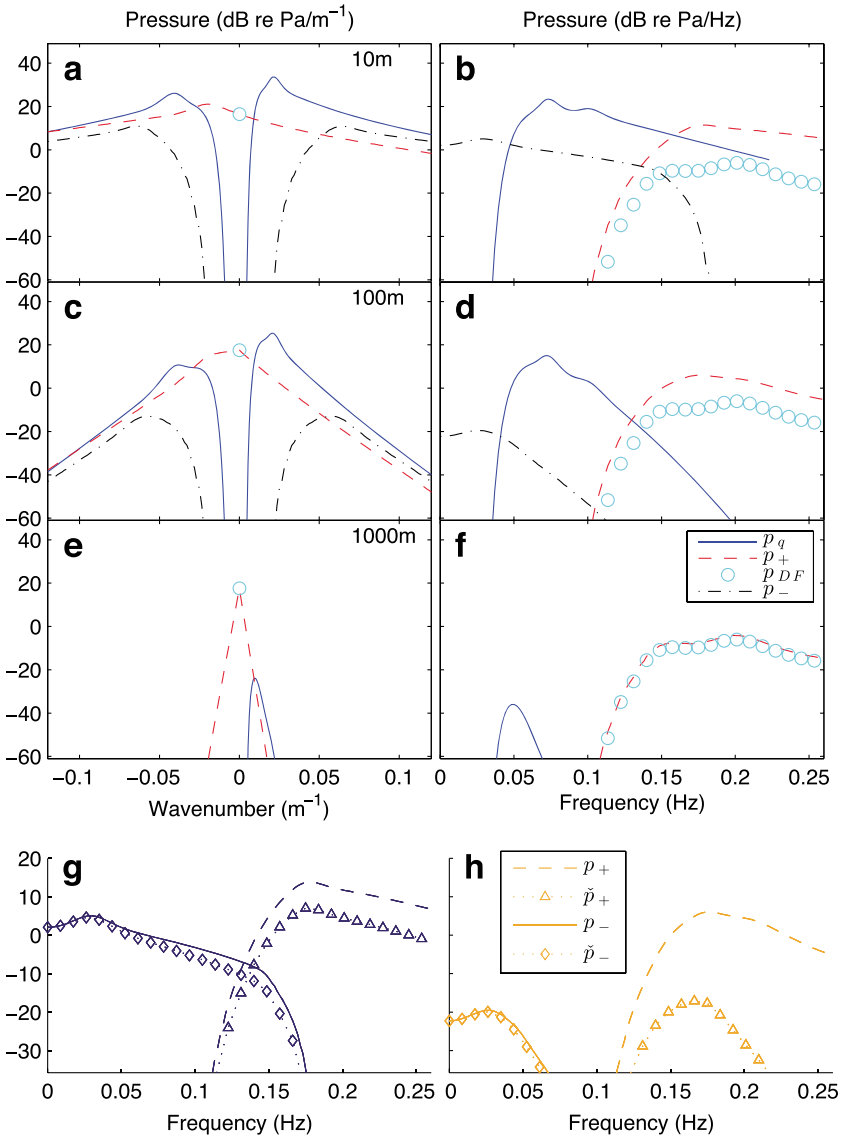

Figure 6. Pressure spectra of the first-order pressure p_q (solid line), and the second-order sum p_+ (dashed line) and difference p_- pressures (dash-dotted line) at depths of (a, b) 10, (c, d) 100, and (e, f) 1000 m. Pressure spectra of $p_\pm$ (dashed, dash-dotted lines) and $\check{p}_\pm$ (triangle, square) (equation (32)) at depths of (g) $z = 10$ and (h) $z = 100$ m.

spectrum [*Hasselmann et al.*, 1973]

$$
\begin{aligned}
a_{\mathbf{q}} &= \frac{\alpha g^2}{\sigma_{\mathbf{q}}^5} 3.3^r e^{-\frac{5}{4}\left(\frac{\sigma_p}{\sigma_{\mathbf{q}}}\right)^4} \\
r &= e^{-\frac{(\sigma_{\mathbf{q}}-\sigma_p)^2}{2\beta^2\sigma_p^2}} \qquad , \quad \alpha = 0.076\left(\frac{U_{10}^2}{Fg}\right)^{0.22} \\
\sigma_p &= 22\left(\frac{g^2}{U_{10}F}\right)^{1/3} \qquad , \quad \beta = \begin{cases} 0.07 & \sigma \le \sigma_p \\ 0.09 & \sigma > \sigma_p \end{cases}
\end{aligned}
\tag{57}
$$

with wind speed U_{10} of 15 and 20 m/s and fetch F of 700 and 200 km. The first-order solutions ϕ_q (equation (10)) were computed as functions of q for 256 equispaced values (1.6×10^{-3} spacing) of q from −0.2 to 0.2 m^{-1}. As the wave spectra have different wind speeds and fetch, they have different peak frequencies (0.07 and 0.1 Hz) but their spectra overlap (Figure 3).

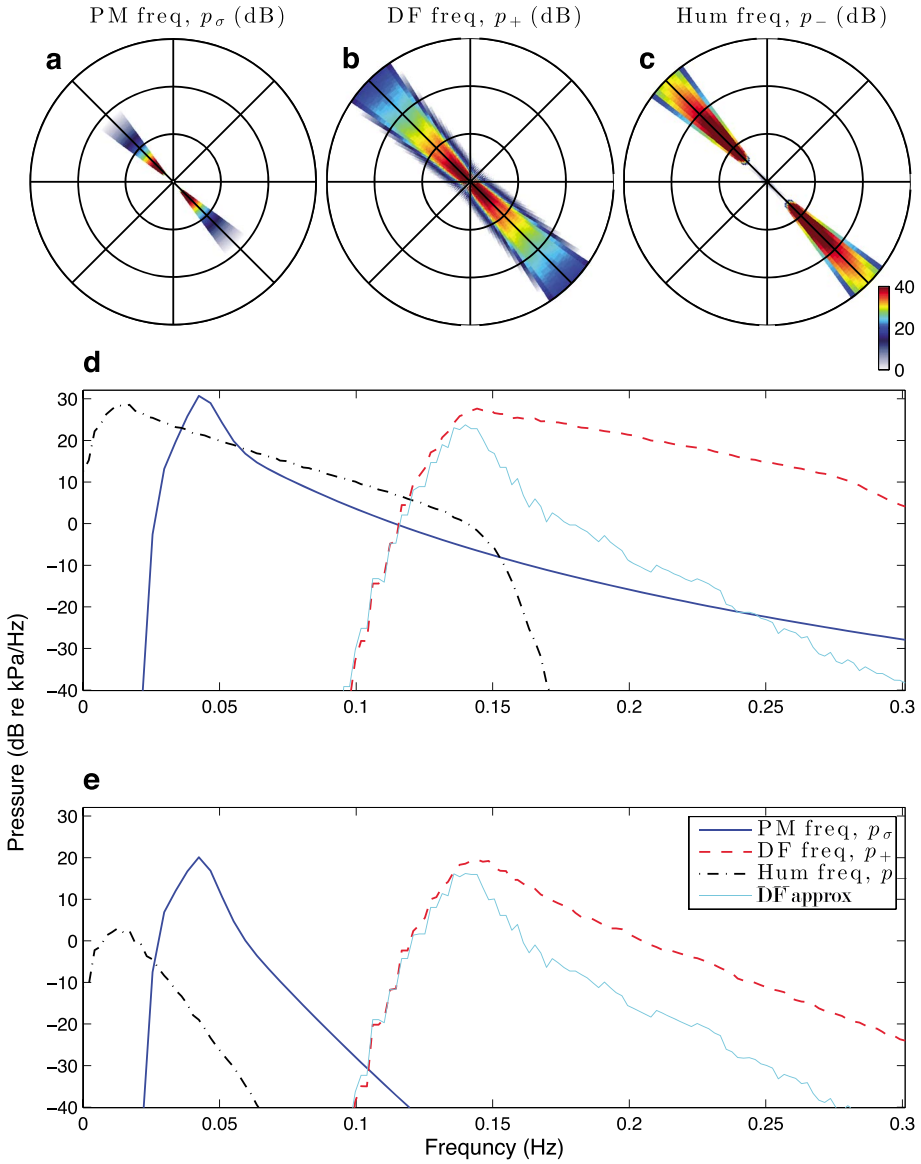

Figure 7. Two-dimensional pressure spectra for (a) first-order, $p_{\mathbf{q}}$, (b) second-order sum, p_+, and (c) second-order difference, p_-, contributions for opposing first-order waves in a compressible ocean of 100 m depth (radial rings: 0.05, 0.1, and 0.15 m^{-1}). The pressure spectra are integrated over all angles and plotted against frequency at the ocean (d) surface and (e) bottom (dB referenced to kPa/Hz).

5.1.2. Numerical Integration

To compute the second-order pressure (equation (30)) the integrals in equation (28) must be evaluated, which we do, numerically. In a 1-D model, $\mathbf{q}$ becomes $\pm|q|$, and from the 256 values of q in our model we compute a 256 × 256 matrix in which the row and column indices correspond to the indices of two interacting spectral components, q_1 and q_2. For each value we compute four matrices of the second-order wave number and frequency produced by sum and difference interactions: $k_+ = q_1 + q_2, k_- = q_1 - q_2$, $\omega_+ = \sqrt{g|q_1|} + \sqrt{g|q_2|}$, and $\omega_- = |\sqrt{g|q_1|} - \sqrt{g|q_2|}|$. The values of these second-order wave numbers and frequencies are contoured over $\{q_1, q_2\}$ space in Figures 4a and 4b. As $\Theta = 0$ for $\theta_{12} = 0$, we only plot the second and fourth quadrants, in which the quadratic interaction (RHS of equation (28)) is nonzero.

Using the JONSWAP spectrum (equation (57)) to compute $a_{\mathbf{q}}$ (and thence $\eta_{\mathbf{q}} = 2a_{\mathbf{q}}$), the integrand of equation (28) is computed over $\{q_1, q_2\}$ space and multiplied by $\rho\omega^2/D$ to give units of pressure (as in equation (30)). This integrand is plotted in Figures 4c and 4d over the region corresponding to the fourth quadrants of Figures 4a and 4b. Note that in the sum interaction (Figure 4c) $\omega = \sqrt{g|q_1|} + \sqrt{g|q_2|}$,

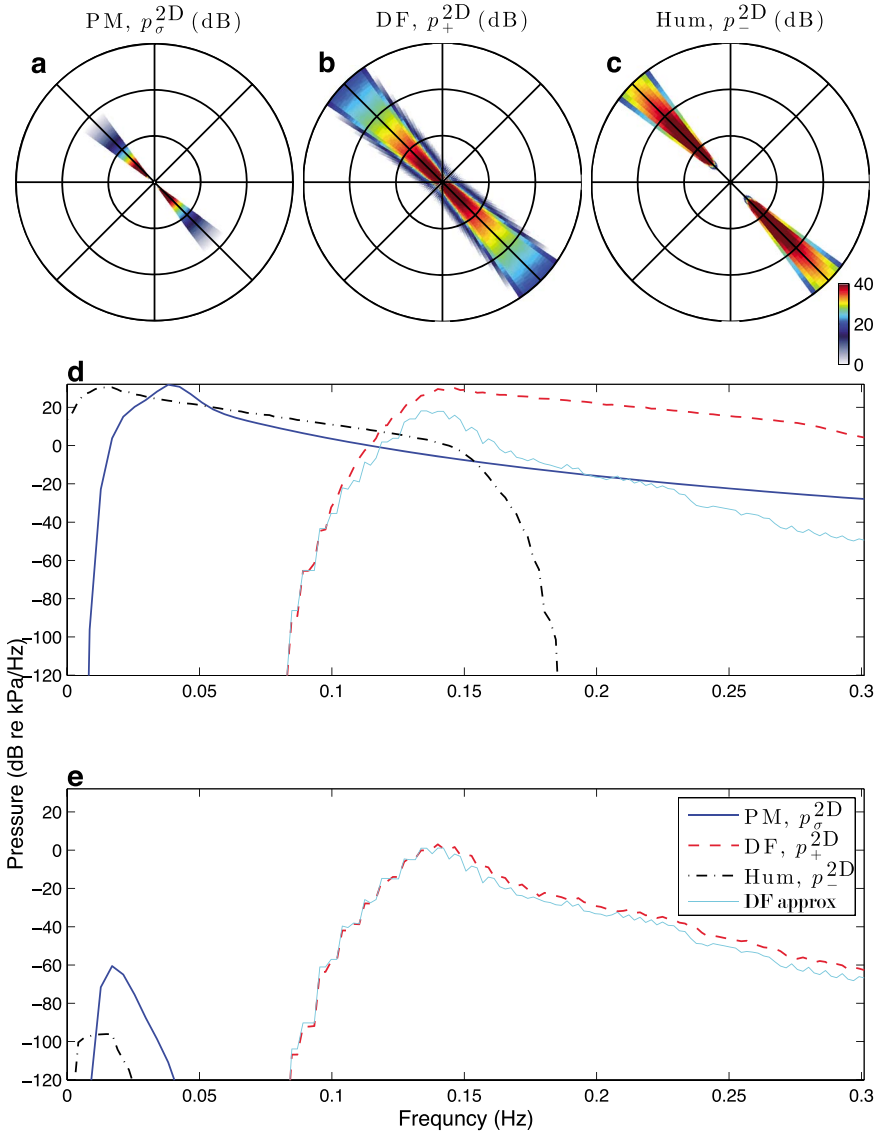

Figure 8. Two-dimensional pressure spectra for (a) first-order, $p_{\mathbf{q}}$, (b) second-order sum, p_+, and (c) second-order difference, p_-, contributions for opposing first-order waves in a compressible ocean of 1000 m depth (radial rings: 0.05, 0.1, and 0.15 m^{-1}). The pressure spectra are integrated over all angles and plotted against frequency at the ocean (d) surface and (e) bottom (dB referenced to kPa/Hz).

whereas in the difference interaction (Figure 4d) $\omega = |\sqrt{g|q_1|} - \sqrt{g|q_2|}|$, and hence, the integrand, which is proportional to ω^2, is zero along the diagonal in the difference interaction. This is the value where $q_1 = -q_2$ and hence is the region where double-frequency standing waves occur (section 3.4).

To compute the second-order pressure spectrum a 513-point equispaced vector of second-order wave number (k) is defined from −0.4 to 0.4 m^{-1} (spacing $\Delta k = 1.6 \times 10^{-3}$ m^{-1}) and a 256-point equispaced vector of second-order frequency ω is defined from 0 to $2\sqrt{0.2g}$ Hz (max = 2.8 Hz, spacing. $\Delta\omega = 0.011$ Hz). For the ith index of wave number k_i and the jth index of frequency ω_i, the indices of the matrices of $k_\pm(q_1, q_2)$ and $\omega_\pm(q_1, q_2)$ (Figures 4a and 4b) are computed for which $k_i - \Delta k < k_\pm < k_i + \Delta k$ and $\omega_j - \Delta\omega < \omega_\pm < \omega_j + \Delta\omega$. The values of the integrand of $S_\pm$ (Figures 4c and 4d) at these indices are collected and summed to compute the integrals in equation (28), and thus, the pressure is computed as a function of k and ω (Figures 4e and 4f).

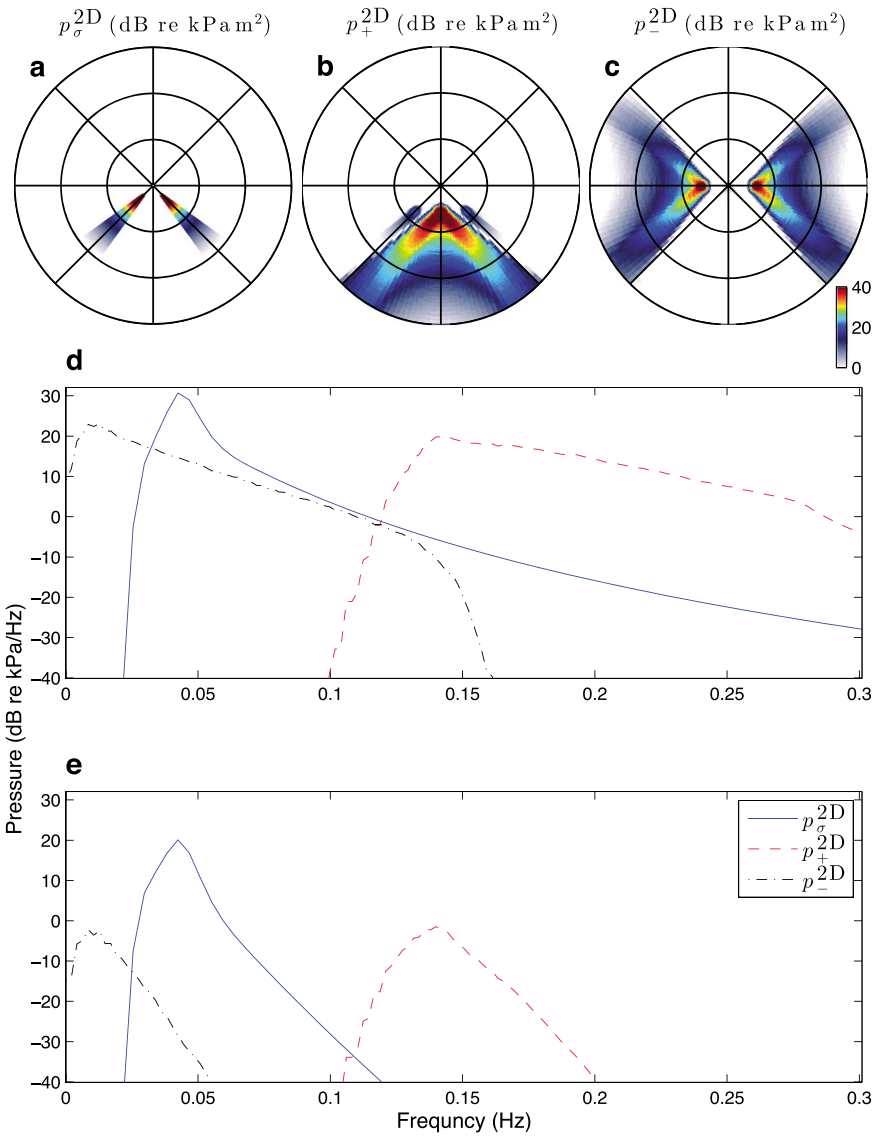

Figure 9. Two-dimensional pressure spectra for (a) first-order, $p_{\mathbf{q}}$, (b) second-order sum, p_+, and (c) second-order difference, p_-, contributions for obliquely interacting first-order waves in a compressible ocean of 100 m depth (radial rings: 0.05, 0.1, and 0.15 m^{-1}). The pressure spectra are integrated over all angles and plotted against frequency at the ocean (d) surface and (e) bottom (dB referenced to kPa/Hz).

5.1.3. Results

The sum pressure occurs at higher frequencies than the difference pressure (Figures 4e and 4f). This difference is accounted for by the differing values of the contours of $\omega_\pm$ over the region of $\{q_1, q_2\}$ space with energy peaks in $\eta_1\eta_2$. Only the sum pressure contains spectral components at $k = 0$.

A similar procedure is performed to compute $\check{S}_\pm$ (equation (31)) which, at the surface ($z = 0$), (where $Z = Z_{\mathbf{k}} = \check{Z} = 1$) differs from $S_\pm$ only in the multiplicative factor. Thus, the sum and difference surface pressures (equation (30)) are computed. Integrating over frequency and wave number, the surface pressure spectra can be plotted as functions of wave number (Figure 5a) and frequency (Figure 5b), respectively. Integrating only over $k = 0$ (performed by keeping only the diagonal elements of the matrices spanning $\{q_1, q_2\}$ space, which is equivalent to integrating only along the dotted lines in Figures 4c and 4d) gives the double-frequency approximation (equation (33)). The peak sum and difference pressures are 10 and 15 dB smaller than the first-order pressures and occur at approximately the sum ($0.1 + 0.07 = 0.17$ Hz) and difference ($0.1 - 0.07 = 0.03$ Hz) of the two peaks in the first-order spectrum. Only the sum pressure yields a nonzero result after integration over the DF approximation.

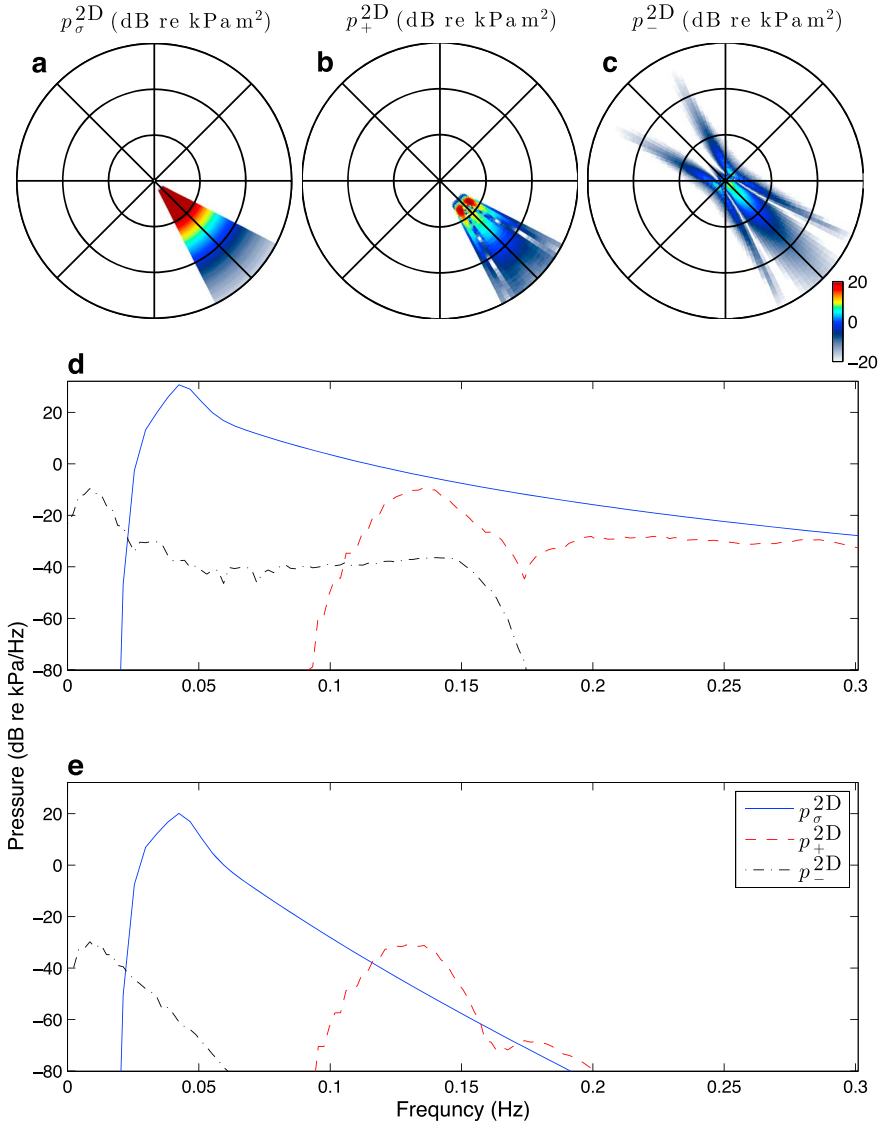

Figure 10. Two-dimensional pressure spectra for (a) first-order, $p_{\mathbf{q}}$, (b) second-order sum, p_+, and (c) second-order difference, p_-, contributions for a single first-order wave in a compressible ocean of 100 m depth (radial rings: 0.05, 0.1, and 0.15 m^{-1}). The pressure spectra are integrated over all angles and plotted against frequency at the ocean (d) surface and (e) bottom (dB referenced to kPa/Hz).

The depth dependance (equations (10) and (30)) is computed by multiplying the matrices defining the integrands of $S_\pm$ (illustrated in Figures 4c and 4d) by $Z_{\mathbf{k}} = e^{-|k_\pm|z}$ and $\check{Z} = e^{-(|q_1|+|q_2|)z}$ before integration (section 5.1.2). This allows the pressure spectrum to be computed at $z = 10$, 100 and 1,000 m (Figure 6). The second-order sum pressure p_+ increases relative to the first-order pressure p_q (Figure 6) with increasing depth and by 1000 m the DF approximation is accurate. The difference pressure p_- decays rapidly, since it peaks at higher k than the first order and sum pressure. The quadratic sum $\check{p}_+$ decays faster with depth than the full-solution p_+ and the quadratic difference $\check{p}_-$ decays similarly to the full-solution p_- (Figure 6g).

5.2. Two-Dimensional Compressible Shallow-Water Ocean

As in section 5.1, we numerically compute the first- and second-order pressures for realistic surface wave spectra; however, in this case we use the compressible equations of section 4, with sound speed $c = 1500$ m/s and ocean depth $H = 100$ m or $H = 1000$ m. We consider three surface wave spectra, all generated with a JONSWAP spectrum with wind speed 20 m/s acting over a fetch of 700 km and with three angular distributions: (1) an opposing wave scenario, in which the spectral wave energy is contained within two 18° azimuth bins that directly oppose each other; (2) an oblique wave scenario, in which the spectral

wave energy is contained within two 18° azimuth bins with centers separated by 90°; and (3) a single wave train scenario, in which the spectral wave energy is contained within one 36° azimuth bin. At all azimuths outside these bins the spectrum is zero. The directional spread of ocean waves is ubiquitous in observations and is often modeled using an azimuthal spread function [*Webb and Cox*, 1986; *Farrell and Munk*, 2010]. We forego this function and directly define the 2-D spectra.

5.2.1. Numerical Integration

The numerical integrations are computed in the same manner as described in section 5.1.2 except the integrands of equation (52) (analogous to those shown in Figures 4c and 4d) are now 4-D tensors over $\{\mathbf{q}_1, \mathbf{q}_2\}$ space and the contours of $|\mathbf{k}_\pm|$, $\omega_\pm$ analogous to Figures 4a and 4b), must be computed over this 4-D space, as do the second-order azimuths [$\theta_\pm = \arctan(k_y/k_x)$], for sum and difference interactions. The first-order spectra were discretized over 100 wave numbers $|\mathbf{q}|$ (1.8×10^{-3} m^{-1} spacing) and 160 azimuth (2.25° spacing) bins. The frequency σ of each wave number bin was computed with the shallow-water dispersion relation (equation (43)). The $|\mathbf{k}_\pm|$, $|\omega_\pm|$ and $\theta_\pm$ were computed for each value of a $100 \times 100 \times 160 \times 160$ tensor encompassing all possible interacting first-order pairs.

For numerical efficiency, the integrals of equation (52) were approximated by identifying the index of the 4-D integrand of $S_\pm$ with maximal power and summing its magnitude into the appropriate bins of second-order sum and difference wave numbers $|\mathbf{k}_\pm|$ (200 bins, 1.8×10^{-3} m^{-1} spacing), frequencies $\omega_\pm$ (100 bins, 1.9×10^{-2} Hz), and azimuths $\theta_\pm$ (160 bins, 2.25° spacing). The summation was continued successively with the next largest component of $S_\pm$ until the net change in power of the second-order spectra (both sum and difference interactions) was more than 160 dB below the spectral peak.

The sum and difference pressure spectra are computed as a function of $\mathbf{k}$ and ω at the surface and at the 100 m seabed and plotted in Figures 7, 9, and 10 for the three surface wave spectra considered. The seabed pressure due to opposing waves is also computed in a deepwater simulation with 1000 m depth (Figure 8).

5.2.2. Results

In the case of opposing waves in 100 m ocean depth (Figure 7) the sum pressure spectrum contains a peak at twice the frequency of the first-order wave spectrum and, at the seabed, this is approximately equal in power to the first-order peak. A portion of the energy contained in the sum-pressure, at wave number $|\mathbf{k}| = 0$ (the DF approximation, section 3.4), will not decay with depth, and this result describes the well known double-frequency standing wave solution. However, the full-pressure spectrum including all evanescent components produces significant differences in seabed pressure, in that it contains (1) more energy than the DF approximation at frequencies above the DF peak (0.14 Hz, Figure 7d) and (2) the difference pressure p_- produces a spectral peak at very low frequencies which, at its peak frequency (0.01 Hz), is equivalent in power to the first-order $p_\mathbf{q}$ and sum p_+ pressure. The frequency of these peaks ($p_\mathbf{q}$, p_+, and p_-) correspond to the frequencies of observed seismic noise (PM, DF, and hum). In this simulation, the sum pressure peak is at $|\mathbf{k}| = 0$, but this is only because the two opposing wave trains are exactly equal and opposite; in general, the sum pressure peak will not be at $|\mathbf{k}| = 0$ (for example, Figure 5a). The same opposing wave surface spectrum was used to compute the pressure response in an ocean of 1000 m depth (Figure 8). In such deepwater cases the DF approximation well approximates the seabed pressure.

In the case of obliquely interacting waves (Figure 9), there is no energy produced at $|\mathbf{k}| = 0$ (Figure 9b); and correspondingly, the sum and the difference pressure spectral peaks at the seabed are both 20 dB lower than the peak of the first-order pressure spectrum, and the DF approximation is zero. In the case of a single wave (Figure 10) spread over a range of azimuths, the sum and difference pressures decay more rapidly with depth and are 50 dB below the first-order pressure.

The obliquely interacting waves and single waves with directional spread produce weaker seabed pressures than the sum pressure produced by opposing waves. Opposing waves, however, require particular sea states, whereas the more general interactions are likely ubiquitous, particularly in shallow water where seabed interactions can diffract and refract incoming waves. Thus, we expect spectral peaks at frequencies corresponding to the sum and difference of ocean waves to be ubiquitous in shallow waters.

6. Conclusion

A full evaluation of second-order pressure spectrum in the water column shows two distinct peaks. One peak is produced by *sum* interactions of the first-order waves and occurs at about double the peak of the first-order spectrum. The second peak is produced by *difference* interactions of the first-order waves and

occurs at much lower frequencies than the first-order wave. The frequency bands of these two peaks are consistent with the observed spectra of DF microseisms and the Earth's seismic hum. The first-order pressure waves produce a spectral peak at frequencies consistent with the observed PM spectrum. At the seabed in shallow water these three spectral peaks are similar in power and, as they are generated by obliquely interacting waves and single waves with an azimuthal spread of energy, they are likely ubiquitous.

Thus, a complete integration of the first-order interactions, including the hitherto ignored difference interactions, is consistent with the standing wave theories in deep water but yields a more complete theory. In *shallow water* this theory suggests the following:

1. Microseisms and hum may be simultaneously generated by the same wave-wave interactions;
2. DF microseism generation may be stronger than predicted by standing wave theories;
3. DF and hum generation can occur in the absence of opposing wave components;
4. A single wave train with a directional spread generates weak microseisms and hum; and
5. Because of (3) and (4) microseisms and hum can be generated without coastal reflections.

Acknowledgments
This work was supported by NSF grants EAR-0710881, EAR-0944109, and OCE-1030022. We gratefully acknowledge Peter D. Bromirski for providing feedback and insight. Additional logistical support was provided by Dan Hammer and Beth Hagen.

References

Ardhuin, F., E. Stutzmann, M. Schimmel, and A. Mangeney (2011), Ocean wave sources of seismic noise, *J. Geophys. Res.*, *116*, C09004, doi:10.1029/2011JC006952.

Ardhuin, F., A. Balanche, E. Stutzmann, and M. Obrebski (2012), From seismic noise to ocean wave parameters: General methods and validation, *J. Geophys. Res.*, *117*, C05002, doi:10.1029/2011JC007449.

Ardhuin, F., and T. H. C. Herbers (2013), Double-frequency noise generation by surface gravity waves in finite depth: Gravity, acoustic and seismic modes, *J. Fluid Mech.*, *716*, 316–348, doi:10.1017/jfm.2012.548.

Brooks, L. A., and P. Gerstoft (2009), Green's function approximation from cross-correlations of 20–100 Hz noise during a tropical storm, *J. Acoust. Soc. Am.*, *125*, 723–734.

Bromirski, P. D., F. K. Duennebier, and R. A. Stephen (2005), Mid-ocean microseisms, *Geochem. Geophys. Geosyst.*, *6*, Q04009, doi:10.1029/2004GC000768.

Bromirski, P. D., and P. Gerstoft (2009), Dominant source regions of the Earth's "hum" are coastal, *Geophys. Res. Lett.*, *36*, L13303, doi:10.1029/2009GL038903.

Cato, D. H. (1991a), Sound generation in the vicinity of the sea surface: Source mechanisms and the coupling to the received sound field, *J. Acoust. Soc. Am.*, *89*, 1076–1095, doi:10.1121/1.400527.

Cato, D. H. (1991b), Theoretical and measured underwater noise from surface wave orbital motion, *J. Acoust. Soc. Am.*, *89*, 1096–1112, doi:10.1121/1.400527.

Cox, C. S., and D. C. Jacobs (1989), Cartesian diver observations of double frequency pressure fluctuations in the upper levels of the ocean, *Geophys. Res. Lett.*, *16*, 807–810.

Duennebier, F. K., R. Lukas, E.-M. Nosal, J. Aucan, and R. A. Weller (2012), Wind, waves, and acoustic background levels at Station ALOHA, *J. Geophys. Res.*, *117*, C03017, doi:10.1029/2011JC007267.

Farrell, W. E., and W. Munk (2008), What do deep sea pressure fluctuations tell about short surface waves?, *Geophys. Res. Lett.*, *35*, L19605, doi:10.1029/2008GL035008.

Farrell, W. E., and W. Munk (2010), Booms and busts in the deep, *J. Phys. Oceanogr.*, *40*, 2159–2169, doi:10.1175/2010JPO4440.1.

Fukao, Y., K. Nishida, and N. Kobayashi (2010), Seafloor topography, ocean infragravity waves, and background Love and Rayleigh waves, *J. Geophys. Res.*, *115*, B04302, doi:10.1029/2009JB006678.

Gerstoft, P., P. M. Shearer, N. Harmon, and J. Zhang (2008), Global P, PP, and PKP wave microseisms observed from distant storms, *Geophys. Res. Lett.*, *35*, L23306, doi:10.1029/2008GL036111.

Harmon, N., D. Forsyth, and S. Webb (2007), Using ambient seismic noise to determine short-period velocities and shallow shear velocities in young oceanic crust, *Bull. Seismol. Soc. Am.*, *97*, 2009–2023, doi:10.1785/0120070050.

Hasselmann, K. (1962), On the non-linear energy transfer in a gravity-wave spectrum. Part 1. General theory, *J. Fluid Mech.*, *12*, 481–500.

Hasselmann, K. (1963), A statistical analysis of the generation of microseisms, *Rev. Geophys.*, *1*, 177–210, doi:10.1029/RG001i002p00177.

Hasselmann, K., et al. (1973), Measurements of wind-wave growth and swell decay during the Joint North Sea Wave Project (JONSWAP), *Dtsch. Hydrogr. Z.*, *12*, suppl. A8, 95 pp.

Haubrich, R. A., and K. McCamy (1969), Microseisms: Coastal and pelagic sources, *Rev. Geophys.*, *7*, 539–571.

Hedlin, M. A. H., K. Walker, D. P. Drob, and C. D. de Groot-Hedlin (2012), Infrasound: Connecting the solid earth, oceans and atmosphere, *Annu. Rev. Earth Planet. Sci.*, *40*, 327–354, doi:10.1146/annurev-earth-042711-105508.

Herbers, T. H. C., and R. T. Guza (1991), Wind-wave nonlinearity observed at the sea floor. Part I: Forced-wave energy, *J. Phys. Oceanogr.*, *21*(12), 1740–1761.

Herbers, T. H. C., and R. T. Guza (1992), Wind-wave nonlinearity observed at the sea floor. II: Wavenumbers and third-order statistics, *J. Phys. Oceanogr.*, *22*(5), 489–504.

Herbers, T. H. C., and R. T. Guza (1994), Nonlinear wave interactions and high-frequency seafloor pressure, *J. Geophys. Res.*, *99*(C5), 10,035–10,048, doi:10.1029/94JC00054.

Herbers, T. H. C., S. Elgar, and R. T. Guza (1995), Generation and propagation of infragravity waves, *J. Geophys. Res.*, *100*, 24,863–24,872, doi:10.1029/95JC02680.

Hillers, G., N. Graham, M. Campillo, S. Kedar, M. Landès, and N. Shapiro (2012), Global oceanic microseism sources as seen by seismic arrays and predicted by wave action models, *Geochem. Geophys. Geosyst.*, *13*, Q01021, doi:10.1029/2011GC003875.

Kedar, S., M. Longuet-Higgins, F. Webb, N. Graham, R. Clayton, and C. Jones (2008), The origin of deep ocean microseisms in the North Atlantic Ocean, *Proc. R. Soc. A*, *464*, 777–793, doi:10.1098/rspa.2007.0277.

Kibblewhite, A. C., and C. Y. Wu (1996), *Wave Interactions As a Seismo-Acoustic Source*, Lecture Notes in Earth Sciences, vol. 59, Springer, Berlin, Germany.

Kobayashi, N., and K. Nishida (1998), Continuous excitation of planetary free oscillations by atmospheric disturbances, *Nature*, *395*, 357–360.

Koper, K. D., K. Seats, and H. M. Benz (2010), On the composition of Earth's short-period seismic noise field, *Bull. Seismol. Soc. Am.*, *100*, 606–617.
Kuperman, W. A., and F. Ingenito (1980), Spatial correlation of surface generated noise in a stratified ocean, *J. Acoust. Soc. Am.*, *67*, 1988–1996.
Landès, M., F. Hubans, N. M. Shapiro, A. Paul, and M. Campillo (2010), Origin of deep ocean microseisms by using teleseismic body waves, *J. Geophys. Res.*, *115*, B05302, doi:10.1029/2009JB006918.
Landès, M., L. Ceranna, A. Le Pichon, and R. Matoza (2012), Localization of microbarom sources using the IMS infrasound network, *J. Geophys. Res.*, *117*, D06102, doi:10.1029/2011JD016684.
Longuet-Higgins, M. S. (1950), A theory of the origin of microseisms, *Philos. Trans. R. Soc. London, Ser. A*, *243*, 1–35.
Nishida, K., and N. Kobayashi (1999), Statistical features of Earth's continuous free oscillations, *J. Geophys. Res.*, *104*, 28,741–28,750, doi:10.1029/1999JB900286.
Nishida, K. (2013), Earth's background free oscillations, *Annu. Rev. Earth Planet. Sci.*, *41*, 719–740, doi:10.1146/annurev-earth-050212-124020.
Obrebski, M. J., F. Ardhuin, E. Stutzmann, and M. Schimmel (2012), How moderate sea states can generate loud seismic noise in the deep ocean, *Geophys. Res. Lett.*, *39*, L11601, doi:10.1029/2012GL051896.
Obrebski, M. J., F. Ardhuin, E. Stutzmann, and M. Schimmel (2013), Detection of microseismic compressional (P) body waves aided by numerical modeling of oceanic noise sources, *J. Geophys. Res. Solid Earth*, *118*, 4312–4324, doi:10.1002/jgrb.50233.
Rhie, J., and B. Romanowicz (2004), Excitation of Earth's continuous free oscillations by atmosphere-ocean-seafloor coupling, *Nature*, *431*, 552–556, doi:10.1038/nature02942.
Rhie, J., and B. Romanowicz (2006), A study of the relation between ocean storms and the Earth's hum, *Geochem. Geophys. Geosyst.*, *7*, Q10004, doi:10.1029/2006GC001274.
Romanowicz, B. (2010), Storms, infragravity waves and possible sources of the Earth's vertical and horizontal hum, *Seismol. Res. Lett.*, *81*(2), 363.
Stutzmann, E., F. Ardhuin, M. Schimmel, A. Mangeney, and G. Patau (2012), Modelling long-term seismic noise in various environments, *Geophys. J. Int.*, *191*, 707–722, doi:10.1111/j.1365-246X.2012.05638.x.
Suda, N., N. Nawa, and Y. Fukao (1998), Earth's background free oscillations, *Science*, *279*, 2089–2091.
Svendsen, I. A. (2006), *Introduction to Nearshore Hydrodynamics*, chap. 14, World Sci., Singapore.
Tanimoto, T., J. Um, K. Nishida, and N. Kobayashi (1998), Earth's continuous oscillations observed on seismically quiet days, *Geophys. Res. Lett.*, *25*, 1553–1556.
Tanimoto, T. (2005), The oceanic excitation hypothesis for the continuous oscillations of the Earth, *Geophys. J. Int.*, *160*(1), 276–288.
Tanimoto, T. (2008), The oceanic excitation hypothesis for the continuous oscillations of the Earth, *Geophys. J. Int.*, *160*, 276–288, doi:10.1111/j.1365-246X.2004.02484.x.
Traer, J., P. Gerstoft, P. D. Bromirski, W. S. Hodgkiss, and L. A. Brooks (2008), Shallow-water seismo-acoustic noise generated by tropical storms Ernesto and Florence, *J. Acoust. Soc. Am.*, *124*, EL170-6, doi:10.1121/1.2968296.
Traer, J., P. Gerstoft, P. D. Bromirski, and P. M. Shearer (2012), Microseisms and hum from ocean surface gravity waves, *J. Geophys. Res.*, *117*, B11307, doi:10.1029/2012JB009550.
Walker, K. T. (2012), Evaluating the opposing-wave interaction hypothesis for the generation of microbaroms in the eastern North Pacific, *J. Geophys. Res.*, *117*, C12016, doi:10.1029/2012JC008409.
Waxler, R., and K. E. Gilbert (2006), The radiation of atmospheric microbaroms by ocean waves, *J. Acoust. Soc. Am.*, *119*, 2651–2664, doi:10.1121/1.2191607.
Webb, S. C., and C. S. Cox (1986), Observations and modeling of seafloor microseisms, *J. Geophys. Res.*, *91*, 7343–7358.
Webb, S. C. (1992), The equilibrium oceanic microseism spectrum, *J. Acoust. Soc. Am.*, *92*, 2141–2158, doi:10.1121/1.405226.
Webb, S. C. (2007), The Earth's 'hum' is driven by ocean waves over the continental shelves, *Nature*, *445*, 754–756, doi:10.1038/nature05536.
Webb, S. C. (2008), The Earth's hum: The excitation of Earth normal modes by ocean waves, *Geophys. J. Int.*, *174*, 542–566, doi:10.1111/j.1365-246X.2008.03801.x.
Wilson, D. K., G. V. Frisk, T. E. Lindstrom, and C. J. Sellers (2003), Measurement and prediction of ultralow frequency, ocean ambient noise off the eastern U.S. coast, *J. Acoust. Soc. Am.*, *113*(6), 3117–3133, doi:10.1121/1.1568941.
Zhang, J., P. Gerstoft, and P. D. Bromirski (2010), Pelagic and coastal sources of P-wave microseisms: Generation under tropical cyclones, *Geophys. Res. Lett.*, *37*, L15301, doi:10.1029/2010GL044288.